The Plant Cell, Vol. 29: 871–889, April 2017, www.plantcell.org

Phosphorylation of WRINKLED1 by KIN10 Results in Its Proteasomal Degradation, Providing a Link between Energy Homeostasis and Lipid Biosynthesis[OPEN]

Zhiyang Zhai, Hui Liu, and John Shanklin[1]

Biology Department, Brookhaven National Laboratory, Upton, New York 11973

ORCID IDs: 0000-0003-3181-1773 (Z.Z.); 0000-0002-6774-8043 (J.S.)

WRINKLED1 (WRI1), a member of the APETALA2 (AP2) class of transcription factors, positively regulates glycolysis and lipid biosynthesis in *Arabidopsis thaliana*. Here, we identify mechanistic links between KIN10, the major SUCROSE NON-FERMENTATION1-RELATED KINASE1 involved in sugar/energy homeostasis, and the posttranslational regulation of WRI1. Transient expression of *WRI1* with *OLEOSIN1* in *Nicotiana benthamiana* stimulates triacylglycerol accumulation, but their coexpression with *KIN10* abrogates this effect by inducing proteasomal degradation of WRI1. While WRI1 lacks canonical KIN10 target sequences, we demonstrated direct KIN10-dependent phosphorylation of WRI1 using purified *Escherichia coli*-expressed components. The resulting phosphorylated WRI1 was more rapidly degraded than native WRI1 in cell-free degradation assays. WRI1 phosphorylation was localized to two variants of the canonical KIN10 recognition sequence, one in each of its two AP2 DNA binding domains. Conversion of the phosphorylation sites at Thr-70 and Ser-166 to Ala resulted in a loss of KIN10-dependent phosphorylation, and when coexpressed with KIN10 the WRI1 double mutant accumulated to 2- to 3-fold higher levels than native WRI1. KIN10-dependent degradation of WRI1 provides a homeostatic mechanism that favors lipid biosynthesis when intracellular sugar levels are elevated and KIN10 is inhibited; conversely, glycolysis and lipid biosynthesis are curtailed as sugar levels decrease and KIN10 regains activity.

INTRODUCTION

Sugars are produced by photosynthesis in source tissues, such as leaves, and transported to sink tissues, such as seeds, in which energy-dense storage lipids in the form of triacylglycerol (TAG) esters are stored. In recent years, great progress has been made in identifying global metabolic and hormonal regulatory networks (Gazzarrini and Tsai, 2015). However, few high-level links have been made between global regulation of sugar metabolism and the production of TAG.

Glucose is the universal fuel of life and biological systems have evolved homeostatic mechanisms to regulate its levels. It is also an ancient and conserved regulatory signaling molecule, the levels of which in plants control gene expression and primary and secondary metabolism, as well as growth and development (Sheen, 2014). Plants have three known glucose-modulated master regulators: HEXOKINASE1, a direct glucose sensor (Moore et al., 2003); the energy sensor kinases KIN10 and KIN11, which are inhibited by sugars (Baena-González and Sheen, 2008); and the TARGET OF RAPAMYCIN kinase, which is activated by glucose (Xiong and Sheen, 2012). Representatives of each of these three classes of regulators are found in both plants and animals, though they have become functionally differentiated through the evolution of interactions with multiple protein partners (Sheen, 2014) in which they serve either as regulators or effectors in global cellular regulatory networks (Smeekens et al., 2010).

Eukaryotes possess conserved energy sensor kinases exemplified by yeast SUCROSE-NON-FERMENTATION1 (SNF1) (Celenza and Carlson, 1986) and the mammalian AMP-ACTIVATED PROTEIN KINASE. SNF1 is represented by two genes in *Arabidopsis thaliana*, *KIN10* (*SnRK1.1*) and *KIN11* (*SnRK1.2*), both of which functionally complement the yeast *snf1* mutant (Alderson et al., 1991; Muranaka et al., 1994). KIN10 and KIN11 are central transcriptional integrators of stress and energy signaling that are repressed by sugars (Baena-González et al., 2007). Both isoforms are found in the nucleus and cytoplasm; KIN10 is expressed constitutively, whereas KIN11 is restricted to a small subset of tissues (Williams et al., 2014). While KIN10 and KIN11's complementation of the yeast *snf1* mutation demonstrates their functional redundancy, recent results suggest that their functions are not completely overlapping because overexpression of KIN10 retards flowering time, whereas overexpression of KIN11 advances it (Williams et al., 2014). Overexpression of KIN10 results in the transcriptional activation and repression of more than 1000 genes, the effects of which are to generally increase catabolism and decrease anabolism (Price et al., 2004). Increased sugar levels mitigate the effects of KIN10, favoring anabolic over catabolic processes. One potential substrate identified for KIN10 is the transcription factor FUSCA3 (FUS3), a member of the B3 transcription factor family that plays important roles in meristems and organ specification in addition to seed maturation and oil accumulation (Tsai and Gazzarrini, 2012). KIN10 stabilizes FUS3, which promotes dormancy while inhibiting germination through cross-regulation of abscisic acid and gibberellin pathways (Gazzarrini and Tsai, 2015). FUS3 controls the expression of many

[1] Address correspondence to shanklin@bnl.gov.
The author responsible for distribution of materials integral to the findings presented in this article in accordance with the policy described in the Instructions for Authors (www.plantcell.org) is: John Shanklin (shanklin@bnl.gov).

www.plantcell.org/cgi/doi/10.1105/tpc.17.00019

target genes including *WRINKLED1* (*WRI1*) (Baud and Lepiniec, 2010), a member of the APETALA2 (AP2)/ethylene-responsive element binding protein subfamily of transcription factors involved in the regulation of carbon partitioning into fatty acid synthesis in seeds (Cernac and Benning, 2004). WRI1 activates genes via binding to AW-box target sites containing the sequence $[CnTnG](n)_7[CG]$, where n represents any nucleotide (Maeo et al., 2009). Many transcription factors contain multiple regions of intrinsic disorder (Liu et al., 2006). Analysis of WRI1 itself identified three such regions (Ma et al., 2015). Mutations in WRI1 cause a severe reduction in carbon flux from sugars to pyruvate in the plastidial glycolytic pathway (Focks and Benning, 1998) and an ~80% decrease in fatty acid content in TAG (Baud et al., 2007), resulting in shrunken seeds with a wrinkled appearance. Transcriptomic analysis showed that WRI1 affects expression of genes involved the late steps of glycolysis and some of those in the plastidial fatty acid biosynthesis pathway (Ruuska et al., 2002; Baud et al., 2007; Maeo et al., 2009). Furthermore, transient overexpression of *WRI1* in *Nicotiana benthamiana* leaves results in the upregulation of transcripts related to plastid uptake and metabolism of phosphoenolpyruvate, fatty acid and oil biosynthesis, and fatty acid degradation, whereas those related to photosynthesis and starch degradation are downregulated (Grimberg et al., 2015). Links between sugar and WRI1 activity have previously been established, via the demonstration that sugar can potentiate the accumulation of lipids when WRI1 is ectopically expressed (Cernac and Benning, 2004; Sanjaya et al., 2011; Kelly et al., 2013). In addition, the transcription of *WRI1* can be mildly upregulated in the presence of very high sugar levels, and WRI1 can activate sugar-responsive promoters (Masaki et al., 2005), though the lack of AW-boxes (Maeo et al., 2009) in these promoters suggests their activation by WRI1 may be indirect.

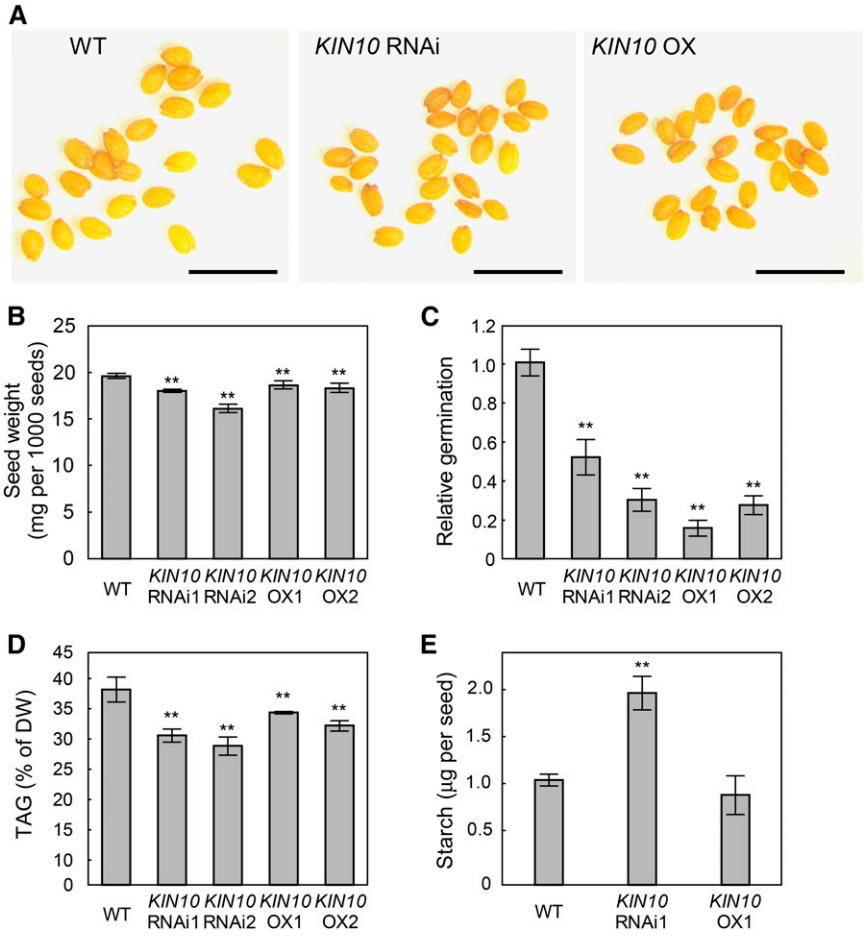

Figure 1. Both *KIN10* OX and RNAi Transgenic Plant Lines Accumulate Lower Levels of TAG in Seeds.

(A) Representative phenotype of seeds of wild type (WT) and *KIN10* RNAi and OX transgenic plants. Bar = 1 mm.
(B) Mean weight of 1000 seeds for wild-type, *KIN10* RNAi (two lines: 1 and 2), and OX plants (two lines: 1 and 2); values represent mean ± SD, $n = 5$.
(C) Relative germination to the wild type (set to 1). Values are mean ± SD of 100 seeds incubated on 0.5× Murashige and Skoog media, $n = 3$.
(D) Seed TAG content; values represent mean ± SD, $n = 5$. DW, dry weight.
(E) Starch quantification in developing seeds (10 d after flowering); values represent mean ± SD, $n = 5$ for each sample of 30 seeds. Asterisks denote statistically significant difference from the wild type (Student's *t* test, **P < 0.01). See Supplemental File 1 for statistical analysis.

Previous reports have demonstrated posttranslational regulation of WRI1 by proteasomal-dependent protein degradation. In one case, the degradation was shown to depend on BTB/POZ-MATH (BPM) (Bric-a-brac/POX virus and zinc finger-meprin and TRAF homology) interactions with WRI1 and the CUL3 E3 ligase (Chen et al., 2013). A C-terminal destabilizing PEST sequence was recently identified, the removal or mutation of which stabilized the Arabidopsis WRI1 (Ma, 2015). More recently, the stabilization of WRI1 has been described upon coexpression with 14-3-3 proteins (Ma et al., 2016), a class of phosphopeptide binding proteins that are conserved within eukaryotes.

In this work, we report that coexpression of *KIN10* with *WRI1* and *OLEOSIN1* (*OLE1*) reduces the lipid accumulation associated with their expression by inducing proteasomal degradation of WRI1. Using purified components, we demonstrate KIN10-dependent phosphorylation of WRI1 and show that the resulting phosphorylated WRI1 is more rapidly degraded than non-phosphorylated WRI1 in cell-free extracts. The WRI1 phosphorylation sites were localized to residues Thr-70 and Ser-166. Coexpression of KIN10 with a WRI1 double mutant in which the phosphorylation sites were converted to Ala resulted in its accumulation to 2- to 3-fold higher levels than wild-type WRI1. The KIN10-dependent degradation of WRI1 identified herein represents a homeostatic mechanism whereby lipid biosynthesis is favored when sugar levels are elevated and KIN10 phosphorylation is inhibited.

RESULTS

Both *KIN10* Overexpression and *KIN10* RNAi Suppression Arabidopsis Transgenic Plant Lines Accumulate Less Oil in Seeds

The observation that *KIN10* overexpression stabilizes FUS3 (Tsai and Gazzarrini, 2012), thereby potentiating seed development and oil accumulation, seems at odds with reports that its overexpression results in poor seed germination (Baena-González et al., 2007). To further investigate this relationship, we performed a detailed phenotypic comparison between wild-type seeds and those of *KIN10*-overexpressing (OX) and RNA interference (RNAi) *KIN10*-suppressed Arabidopsis lines (Baena-González et al., 2007). Visual inspection showed that wild-type seeds were regular in shape, whereas *KIN10*-RNAi and *KIN10*-OX seeds appeared smaller and less symmetrical (Figure 1A). The mean dry weight of wild-type seeds was 19.6 μg, whereas *KIN10*-OX seeds showed a small but significant decrease to 18.3 μg per seed, and the *KIN10*-RNAi line showed a significant decrease, at 17.1 μg per seed (Figure 1B). Germination of both *KIN10*-OX and *KIN10*-RNAi lines was strongly impaired relative to the wild type, with 60% or fewer of the seeds germinating on 0.5× Murashige and Skoog agar plates (Figure 1C). Compositional analysis showed that wild-type seeds contained 35% TAG by dry weight, whereas *KIN10*-OX and *KIN10*-RNAi seeds showed significant reductions in TAG, at 30 and 29% of dry weight, respectively (Figure 1D). That both overexpression and suppression of *KIN10* cause reductions in TAG suggests that KIN10 plays at least two distinct roles in regulating oil biosynthesis. Previous reports have shown that

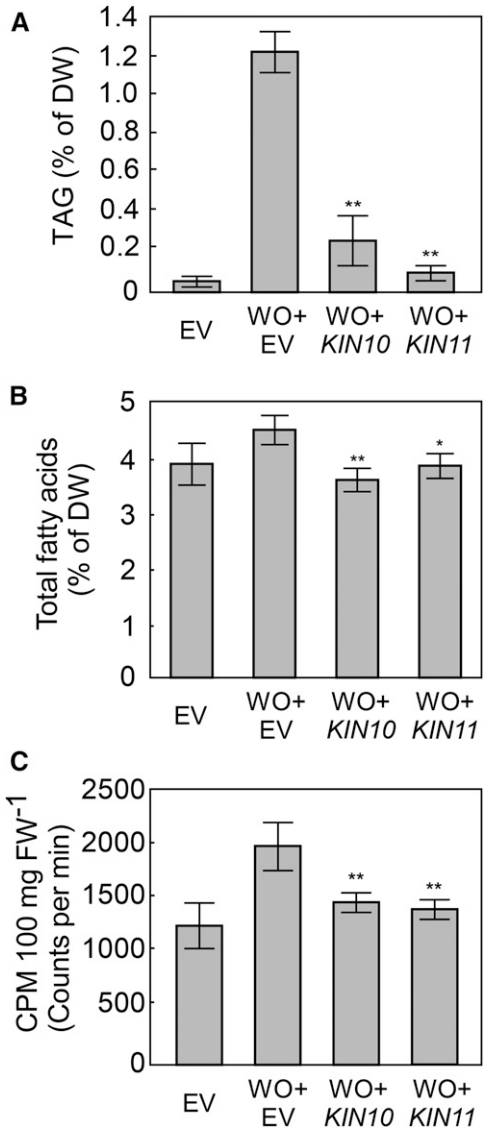

Figure 2. Overexpression of *KIN10* or *KIN11* Represses Fatty Acid Biosynthesis and Decreases TAG Levels in Leaves.

(A) TAG content in *N. benthamiana* leaves transiently expressing different gene combinations as indicated: EV, empty vector; WO+EV, *WRI1*, *OLE1*, and EV; WO+KIN10, *WRI1*, *OLE1*, and *KIN10*; WO+KIN11, *WRI1*, *OLE1*, and *KIN11*. Values represent mean ± SD, $n = 4$. DW, dry weight.

(B) Total fatty acid quantification in *N. benthamiana* leaves. Values represent mean ± SD, $n = 6$.

(C) [1-^{14}C] Acetate incorporation into fatty acyl products by strips of 5-week-old *N. benthamiana* leaves 3 d after infiltration with genes as indicated. Values represent mean incorporation ± SD ($n = 5$) after 30 min of labeling. Asterisks denotes statistically significant differences from the WO+EV treatment (Student's *t* test, *$P < 0.05$ and **$P < 0.01$).

KIN10 is involved in starch mobilization in leaves (Baena-González et al., 2007). We therefore compared the starch content of wild-type seeds with those of *KIN10*-OX and *KIN10*-RNAi. Suppression of *KIN10* in *KIN10*-RNAi seeds resulted in a doubling of the starch content relative to the wild type, from ~5 to ~10%, whereas

overexpression of *KIN10* did not significantly change seed starch levels relative to the wild type (Figure 1E).

Overexpression of *KIN10* or *KIN11* in *N. benthamiana* Leaves Represses WRI1-Induced Fatty Acid Biosynthesis, Resulting in Reduced TAG Accumulation

To identify factors that can enhance TAG accumulation in plant vegetative tissues, we transiently coexpressed genes in *N. benthamiana* leaves along with *WRI1* and *OLE1* (*WO*). Because KIN10 and KIN11 stabilize FUS3, we coexpressed them individually with WO (Supplemental Figure 1) and monitored leaves for changes in TAG accumulation. Both *KIN10* and *KIN11* coexpression with WO resulted in significant reductions in TAG accumulation relative to that resulting from the expression of *WO* alone. Indeed, TAG levels upon *KIN10* or *KIN11* coexpression with *WO* were close to those of leaves transformed with the empty vector (EV; non-*WO*) control. Specifically, TAG content in leaves cotransformed with *WO* and *KIN10* was 83% lower than in leaves with *WO* and EV (Figure 2A). Similarly, total fatty acids in leaves coexpressing *WO* and *KIN10* was 22% lower than in leaves co-expressing *WO* and EV (Figure 2B). Considering there were very low levels of TAG in wild-type leaves, or in leaves transformed with EV, the expression of *KIN10* or *KIN11* almost completely abolished the stimulatory effect of *WO* on oil accumulation (Figure 2A).

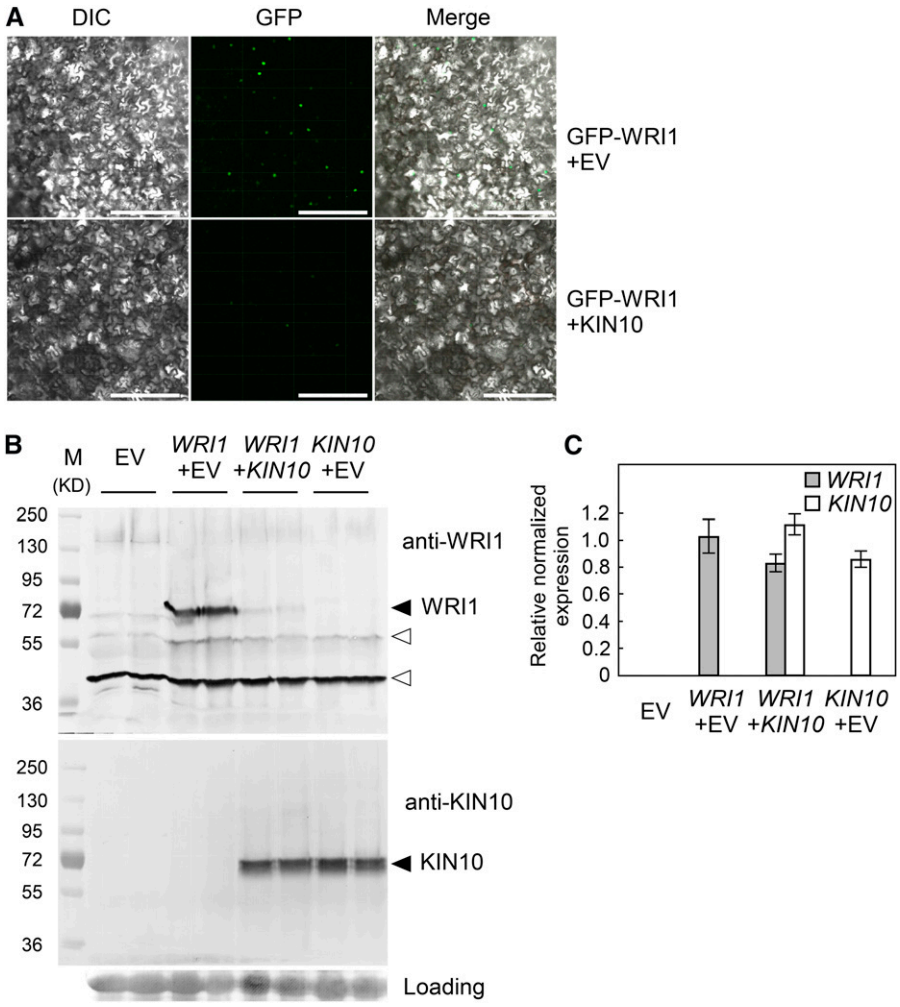

Figure 3. Overexpression of *KIN10* Results in WRI1 Degradation in *N. benthamiana* Leaves.

(A) Representative differential interference contrast (DIC) and fluorescence confocal images of *N. benthamiana* leaf samples 2 d after agroinfiltration with constructs for *GFP-WRI1* expression either alone or with *KIN10*. Bar = 250 μm.

(B) Immunoblot analysis of extracts of *N. benthamiana* leaf extracts 2 d after agroinfiltration to express *WRI1* and EV, *WRI1* and *KIN10*, or *KIN10* and EV. Duplicate blots were probed with anti-WRI1 or anti-KIN10 antibodies. Ponceau S staining of Rubisco is shown as a loading control. M indicates protein markers; solid arrowheads indicate WRI1 or KIN10; open triangles indicate nonspecific signals.

(C) RT-qPCR showing the expression levels of *WRI1* and *KIN10* relative to the *N. benthamiana F-box* gene for the samples analyzed in **(B)**. Values represent mean ± SD (n = 3) using mean crossing point deviation analysis computed by the relative expression (REST) software algorithm.

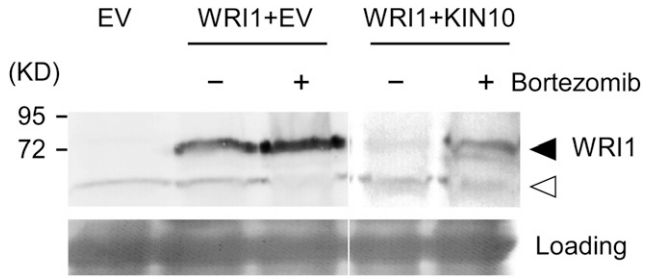

Figure 4. The Proteasome Inhibitor Bortezomib (PS-341) Reduces WRI1 Degradation in Both *WRI1*-Transformed and *WRI1-KIN10*-Cotransformed *N. benthamiana* Leaves.

Leaves were agroinfiltrated to express *WRI1* alone or with *KIN10*. Three days after agroinfiltration, buffer containing (+) or lacking (−) 0.1 μM bortezomib was infiltrated into the leaves, which were harvested 12 h later. Solid arrowheads indicate WRI1. Ponceau S staining of Rubisco is shown as a loading control. Open arrowhead indicates nonspecific signal.

To test whether suppression of TAG accumulation upon the coexpression of *KIN10* or *KIN11* with *WO* resulted from decreased de novo fatty acid biosynthesis, we performed [1-^{14}C] acetate labeling studies in *N. benthamiana* leaves. The rate of fatty acid biosynthesis in leaves coexpressing *WO* with *KIN10* or *KIN11* was 26% lower than in leaves coexpressing *WO* and EV and was not significantly different from leaves expressing the EV control (Figure 2C), demonstrating that *KIN10* overexpression abrogates the increase in fatty acid biosynthesis that resulted from ectopic expression of *WRI1* and *OLE1* in leaves.

Overexpression of *KIN10* Facilitates WRI1 Degradation in *N. benthamiana* Leaves

One possible explanation for the observed neutralization by *KIN10* of the TAG enhancement induced by ectopic expression of *WRI1* and *OLE1* in leaves is that KIN10 facilitates the degradation of WRI1. To test this hypothesis, GFP was fused to the N terminus of WRI1 to facilitate its visualization in vivo via confocal microscopy. When expressed in *N. benthamiana* leaves, GFP-WRI1 resulted in an ~10-fold stimulation of TAG accumulation, demonstrating that fusion of an N-terminal GFP to WRI1 did not substantially change its activity (Supplemental Figure 2B). The GFP signal was localized to the nucleus (Supplemental Figure 2A). Coexpression of *KIN10* along with *GFP-WRI1* in *N. benthamiana* leaves resulted in a decrease in the observable GFP signal (Figure 3A). To detect unmodified WRI1 protein, WRI1 antibody was raised in rabbit. The WRI1 antibody specifically reacted with WRI1 as demonstrated for *Escherichia coli* -expressed WRI1 (Supplemental Figures 3A and 3B); the Coomassie-stained band corresponding to *E. coli*-expressed WRI1 showed mobility of ~72 kD, significantly higher than its predicted molecular mass of 48.4 kD, consistent with its high (15.3%) composition of acidic residue (Graceffa et al., 1992; Alves et al., 2004). As described below, when expressed in *N. benthamiana*, WRI1 showed the same mobility on SDS-PAGE as *E. coli*-expressed protein (Figure 3B). Due to high identity (85%) between Arabidopsis and *Brassica napus* WRI1 (BnWRI1), our AtWRI1 antibody was also reactive with BnWRI1, as demonstrated in *B. napus* embryo derived suspension cells (Supplemental Figure 3C) (Andre et al., 2012).

The anti-WRI1 antibody was used to analyze extracts from leaves expressing *WRI1* alone or with *KIN10*. Strong WRI1 immunoreactive signal was observed for the sample in which *WRI1* was expressed alone, but upon coexpression with *KIN10*, WRI1 was barely detectable (Figure 3B, upper panel). As expected (because endogenous WRI1 expression is predominantly seed specific), no WRI1 signal as detected in empty vector controls or when *KIN10* was expressed alone. RT-qPCR analysis showed that *WRI1* expression was not significantly affected upon its coexpression with *KIN10* (Figure 3C), supporting the conclusion that *KIN10* expression leads to the degradation of WRI1. KIN10

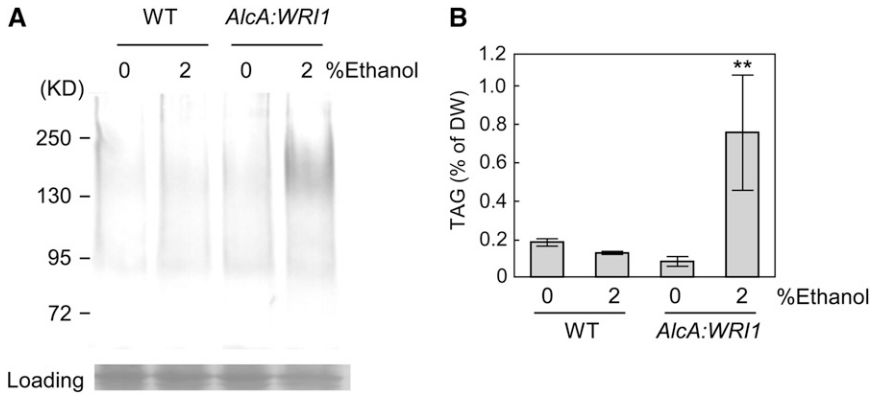

Figure 5. WRI1 Is Represented by an Ensemble of Molecular Masses in Arabidopsis.

(A) Immunoblot analysis using anti-WRI1 antibody on extracts of Arabidopsis leaves expressing *WRI1* under the control of the ethanol-inducible *AlcA* promoter and leaves from control wild-type plants. Plants were irrigated with 2% ethanol (2%) or water (0%) as a negative control. Leaves were harvested 1 week after induction. Ponceau S staining of Rubisco is shown as a loading control.

(B) Leaf TAG content for samples analyzed in **(A)**. Values represent mean ± SD, $n = 6$. Asterisks denote statistically significant difference between controls and ethanol-treated samples (Student's *t* test, **$P < 0.01$). DW, dry weight.

accumulation was confirmed by immunoblotting with commercially available anti-KIN10 antibody (Agrisera).

Specific protein degradation in plants commonly involves proteasomal degradation (Vierstra, 2009). To test whether KIN10-dependent degradation of WRI1 proceeds via the proteasome pathway, we tested whether the potent proteasomal inhibitor bortezomib (PS-341), which binds to the N-terminal Thr residue of the β1 subunit within the 26S proteasome (Shirley et al., 2005), would result in increased WRI1 accumulation. To achieve this, *WRI1* was expressed alone or with *KIN10*, in the presence or absence of bortezomib. Immunoblots of leaf extracts probed with anti-WRI1 antibody showed that under both experimental regimes, levels of WRI1 were increased in the presence of the bortezomib, consistent with the hypothesis that WRI1 is degraded by a proteasomal pathway (Figure 4).

WRI1 Accumulates as an Ensemble of Molecular Masses When Expressed in Arabidopsis Leaves

The analyses described above were performed using transient expression in *N. benthamiana* leaves. We next sought to create stable transgenic *WRI1*-expressing Arabidopsis to further investigate WRI1 degradation. However, ectopic expression of *WRI1* can lead to undesired side effects (Yang et al., 2015). While we were unsuccessful in generating 35S:*WRI1* plants in wild-type Arabidopsis, we were successful in generating stable Arabidopsis *WRI1*-expressing lines in which *WRI1* was placed under the control of an alcohol-inducible promoter (Maizel and Weigel, 2004). After ethanol induction, instead of the single defined band at ~72 kD like that observed when WRI1 was expressed in *N. benthamiana* leaves, *E. coli*, or *B. napus* embryo-derived cell culture, an ensemble of immunoreactive bands of higher molecular mass were observed in leaves of WRI1-expressing Arabidopsis (Figure 5A). Evidence that the expressed WRI1 was active came from TAG measurements showing that relative to uninduced leaves, induction of *WRI1* resulted in an ~8-fold increase in TAG accumulation (Figure 5B). The ensemble of WRI1- immunoreactive signal was also detected in wild-type Arabidopsis siliques (Figure 6A) and Arabidopsis suspension cells (Supplemental Figure 3C). Together, these data suggest that WRI1 in Arabidopsis accumulates in a heretofore uncharacterized posttranslationally modified form.

Arabidopsis Seeds Contain WRI1-Ubiquitin Conjugates

One candidate for creating an ensemble of high molecular weight forms of a protein is via covalent conjugation to the

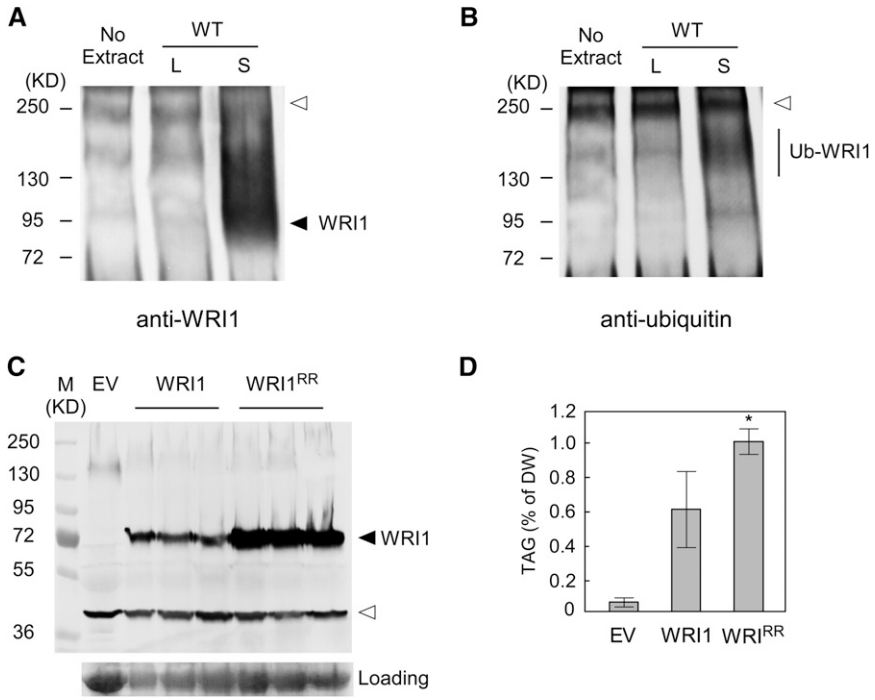

Figure 6. WRI1 Is Ubiquitinated in Arabidopsis.

(A) and **(B)** WRI1 was immunoprecipitated by WRI1 antibody and protein G Sepharose from wild-type Arabidopsis leaves (L) and siliques (S; 10 d after flowering) and blotted with either WRI1 antibody **(A)** or ubiquitin antibody **(B)**. No extract: no tissue extract was added to immunoprecipitation buffer to reveal antibody background. Open triangles indicate nonspecific bands. Ub-WRI1, ubiquitinated WRI1.

(C) A lysine-to-arginine WRI1 mutant ($WRI1^{RR}$, K2R-K3R) was more stable in *N. benthamiana* leaf transient expression assay. For both native and mutant WRI1, proteins from three independently infiltrated leaves are shown.

(D) Expression of a lysine-to-arginine WRI1 mutant resulted in more TAG accumulation than native WRI1. Values are mean ± SD of measurements in *N. benthamiana* leaves 3 d after infiltration, $n = 4$. Asterisk denotes statistically significant difference from native WRI1 (Student's t test, *$P < 0.05$). DW, dry weight.

small protein ubiquitin, a modification that can tag proteins for selective degradation (Hua and Vierstra, 2011). To explore this possibility, WRI1 was recovered from leaves and developing seeds by immunoprecipitation. Duplicate immunoblots of the immunopurified WRI1 were probed with either anti-WRI1 or antiubiquitin antibodies (Figure 6). Anti-WRI1 antibodies revealed a strong heterogeneous ensemble of WRI1 from developing seeds but little from leaves (Figure 6A), consistent with its known expression pattern. Anti-ubiquitin antibodies (Figure 6B) revealed an ensemble of ubiquitin-immunoreactive species that corresponded to a fraction of the higher molecular mass region of the ensemble visualized with the anti-WRI1 antibodies.

Conversion of WRI1 Lysines 2 and 3 to Arginine Residues Increases WRI1 Accumulation in *N. benthamiana*

The identification of high molecular weight WRI-ubiquitin conjugates prompted us to investigate the location of the ubiquitination target sites. Sequence inspection of the WRI1 revealed a dilysine motif at amino acid positions 2 and 3 of WRI1 (Supplemental Figure 4A), i.e., at its N terminus, which is a region of the protein commonly associated with degradation signals (Tasaki et al., 2012). The occurrence of one or two lysine residues in these positions within WRI1 was conserved in several species (Supplemental Figure 4A). To test the hypothesis that these residues are related to WRI1 degradation, we created a mutant WRI1^{RR} in which we replaced the two lysines with arginine

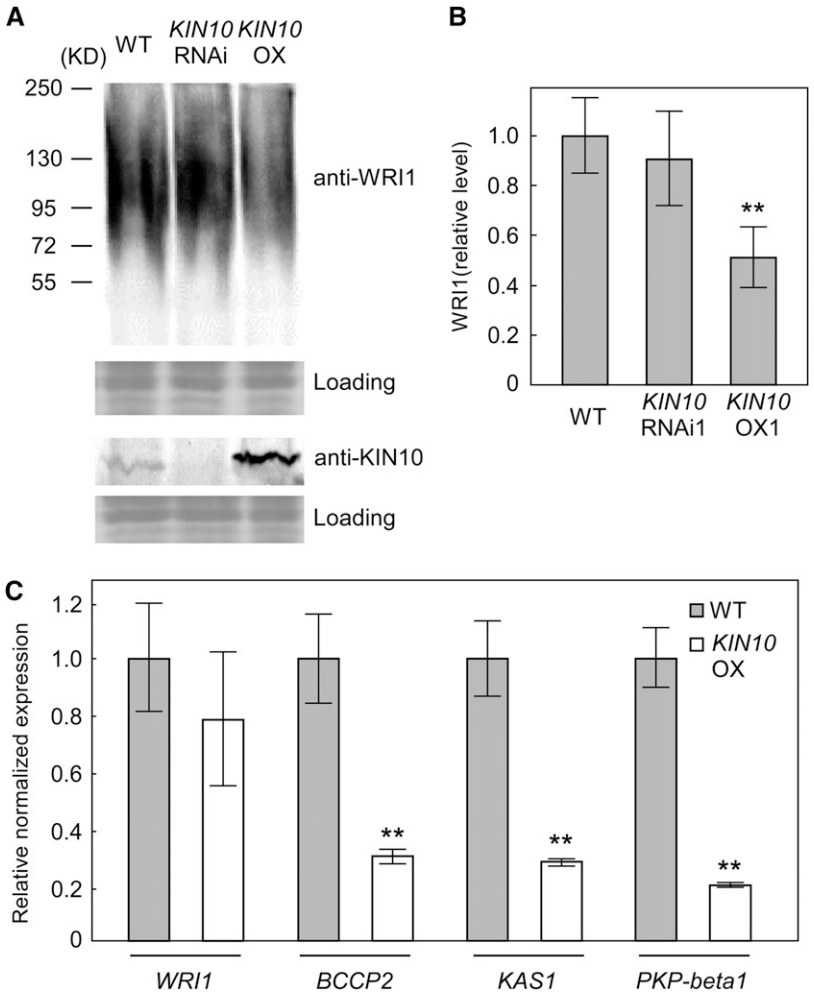

Figure 7. Overexpression of *KIN10* Reduces WRI1 Levels in Siliques.

(A) Immunoblot of seed extracts harvested 10 d after flowering probed with anti-WRI1 or anti-KIN10 antibodies as indicated. Ponceau S staining of Rubisco is shown as a loading control.

(B) Quantification of signal from immunoblots probed with anti-WRI1 antibodies; values represent mean ± SD (n = 3). Wild-type values set to 1.

(C) Expression levels of *WRI1* and three of its target genes: *BCCP2*, *KAS1*, and *PKP-β1*. Values are mean ± SD (n = 3) from three independent experiments. Expression of each gene in the wild type was set to 1. For each experiment, total RNA was isolated from pooled siliques (10 d after flowering) from *KIN10* OX and wild-type plants. Asterisk denotes statistically significant difference from the wild type (using mean crossing point deviation analysis computed by the relative expression [REST] software algorithm; **P < 0.01).

residues, thereby maintaining the positive charge of the native N terminus. When expressed in *N. benthamiana*, WRI1 and WRI1^{RR} expression levels were equivalent (Supplemental Figure 4B). Consistent with our hypothesis, WRI1^{RR} accumulated to significantly higher levels than native WRI1 (Figure 6C), and TAG accumulation increased by ~65% (Figure 6D).

Overexpression of *KIN10* Reduces WRI1 Levels in Arabidopsis Seeds

As visualized by immunoblot (Figure 7A), levels of KIN10 in developing seeds of the Arabidopsis *KIN10*-OX line were approximately an order of magnitude higher than those in wild-type seeds, and KIN10 was not detected in *KIN10*-RNAi suppression lines (Figure 7A). Quantification of the ensemble of WRI1-immunoreactive signal showed that the *KIN10*-overexpressing line contained approximately half that of wild-type and *KIN10*-RNAi suppression lines (Figure 7B).

Analysis of *WRI1* transcript abundance by qPCR in developing seeds of the wild type versus *KIN10*-overexpressing lines showed no significant difference, suggesting that WRI1 protein levels are controlled post transcriptionally, consistent with the degradation observed upon coexpression of *WRI1* and *KIN10* in *N. benthamiana* leaves described above. By contrast, the levels of transcripts for three selected WRI1 target genes, *BCCP2*, *KAS1*, and *PKP-β1* (Maeo et al., 2009), were significantly reduced in the *KIN10*-overexpressing line relative to the wild type (Figure 7C), consistent with the reduced level of WRI1 (Figure 7B).

Kinase Activity Is Essential for KIN10-Dependent WRI1 Degradation

To further study the mechanism of KIN10-dependent WRI1 degradation, two mutants with reduced kinase activity, KIN10 T175A and K48M, were obtained. Phosphorylation of the conserved Thr-175 residue in the activation loop of the kinase domain promotes KIN10 activity, whereas Lys-48 is located within the ATP binding motif; both T175A and K48M mutations inhibit autophosphorylation of KIN10 and thereby reduce its kinase activity (Shen et al., 2009). To test whether KIN10 kinase activity is necessary for KIN10-dependent WRI1 degradation, either native *KIN10* or *KIN10(T175A)* or *KIN10(K48M)* was transiently coexpressed with *WRI1* in *N. benthamiana*. As expected, coexpression of native *KIN10* with *WRI1* resulted in almost complete loss of WRI1 (Figure 8). By contrast, coexpression with either of the *KIN10* mutants resulted in only partial loss of WRI1 (Figure 8). This result demonstrates that KIN10 kinase activity is necessary for the observed KIN10-dependent degradation of WRI1. According to published reports (Crozet et al., 2016), the KIN10 mutants are more stable than native KIN10, explaining their increased accumulation relative to wild-type KIN10 (Figure 8) when expressed in *N. benthamiana*.

Phosphorylated WRI1 Can Be Detected in Native Systems

Because KIN10 kinase activity is necessary for WRI1 degradation, we looked for evidence of possible WRI1 phosphorylation in vivo. We employed phosphate affinity SDS-PAGE with acrylamide-pendant phos-tag (Mn^{2+}-phos-tag), which retards the mobility of phosphorylated polypeptides, enabling separation from their corresponding native forms (Kinoshita et al., 2006). Protein extracts from *N. benthamiana* leaves expressing *WRI1* were separated on either conventional SDS-PAGE or Mn^{2+}-phos-tag gels, prior to immunoblot analysis using anti-WRI1 antibody (Figures 9A and 9B). Following separation by SDS-PAGE, WRI1 signal was observed as a single polypeptide species (Figure 9A). By contrast, upon separation by Mn^{2+}-phos-tag gel, immunoblot analysis revealed two bands, one with the mobility corresponding to that of native WRI1, the other a slower-migrating form that represented a potentially phosphorylated form of WRI1 (Figure 9B). The identity of the slower-migrating form as phosphorylated WRI1 was confirmed by treatment of the extract with alkaline phosphatase prior to gel loading, which converted the slower-migrating form into the faster-migrating native form (Figure 9B). We also performed the experiment with WRI1 that was coexpressed with KIN10, a condition that we would expect to increase the accumulation of phosphorylated WRI1. However, consistent with our findings shown in Figures 3 and 4, coexpression of *KIN10* with *WRI1* reduced the level of WRI1 polypeptide to below detection levels.

We next explored whether phosphorylated WRI1 could be detected in a system unperturbed by exogenous gene expression. To test whether phosphorylated WRI1 can be detected in seed tissue, protein extracts from *B. napus* embryo-derived suspension cell culture were separated using SDS-PAGE and Mn^{2+}-phos-tag gels (Figures 9C and 9D). Immunoblotting of samples separated by SDS-PAGE revealed that, in contrast to the heterogeneous ensemble of immunoreactive species seen in Arabidopsis, WRI1 expressed in *E. coli*, *N. benthamiana*, and *B. napus* cells was observed as single well-defined protein species (Figure 9C). However, when separated via Mn^{2+}-phos-tag gel (Figure 9D), *B. napus* WRI1 contained a slower-migrating species similar to that seen upon the expression of Arabidopsis *WRI1* in *N. benthamiana* (Figures 9B and 9D). As expected, the slower migrating form was absent from *E. coli*-expressed WRI1 (Figure 9D). Thus, phosphorylated forms of WRI1 can be detected in vivo in both *B. napus* and *N. benthamiana*. The observation that a higher proportion of WRI1 is phosphorylated in *N. benthamiana* versus *B. napus*

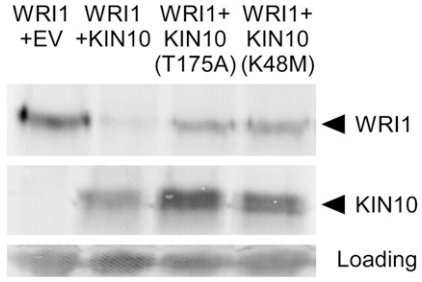

Figure 8. Kinase Activity Is Necessary for KIN10-Dependent WRI1 Degradation.

Immunoblots visualized with anti-WRI1 or anti-KIN10 antibody of extracts from *N. benthamiana* coexpressing *WRI1* with either wild-type *KIN10* or *KIN10(T175A)* or *KIN10(K48M)* that exhibit reduced activity. Ponceau S staining of Rubisco is shown as a loading control.

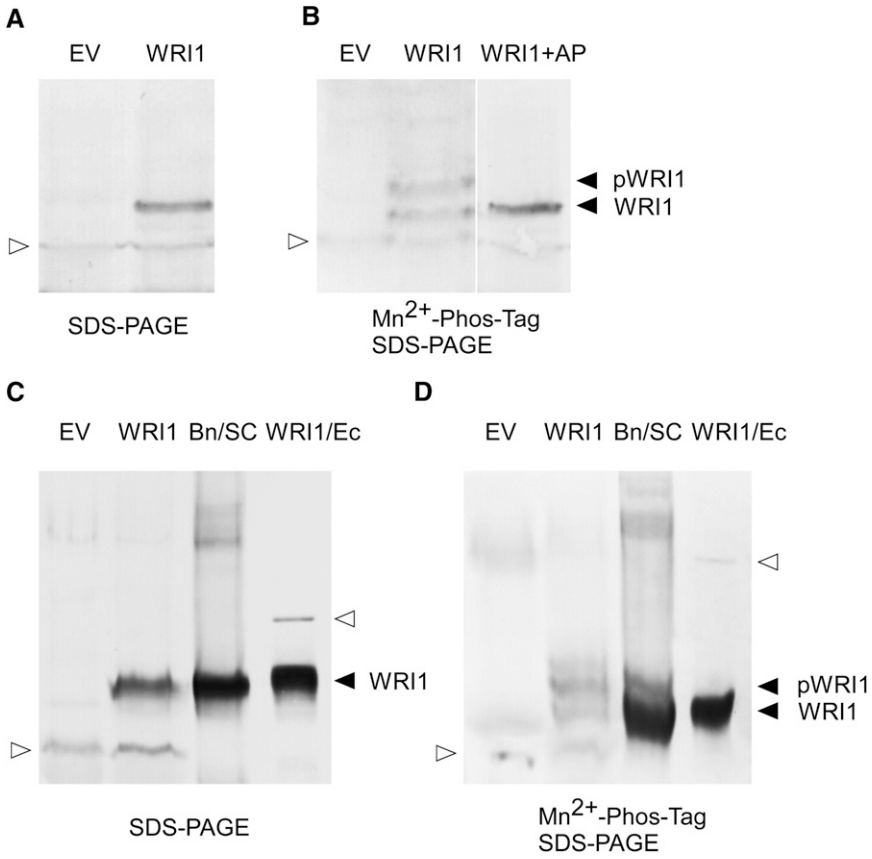

Figure 9. Phosphorylated WRI1 Can Be Detected in Extracts of *N. benthamiana* Leaves and *B. napus* Seeds.

(A) and **(B)** Anti-WRI1 immunoblots of WRI1 expressed in *N. benthamiana* leaves; proteins were separated by SDS-PAGE **(A)** or Mn^{2+}-phos-tag gel electrophoresis **(B)**. *N. benthamiana* leaf samples were harvested 3 d after agroinfiltration with EV or WRI1. WRI1+AP sample was treated with alkaline phosphatase before electrophoresis.

(C) and **(D)** Anti-WRI1 immunoblots of extracts as indicated. Bn/SC, *B. napus* embryo-derived suspension cell; WRI1/Ec, *E. coli* cells expressing *WRI1*. Proteins were separated by SDS-PAGE **(C)** or Mn^{2+}-phos-tag gel electrophoresis **(D)**. Open triangles indicate nonspecific signals.

(Figures 9B and 9D) may reflect their roles as non-oil-accumulating versus oil-accumulating tissues, respectively, in that WRI1 degradation would be expected to be higher in leaf tissue relative to seed tissue.

KIN10 and KIN11 Interact with WRI1

The observations that kinase activity of KIN10 is critical to KIN10-dependent degradation and that WRI1 is phosphorylated implies that either KIN10 interacts directly with WRI1, or the interaction is indirect and one of the many hundreds of KIN10 targets phosphorylates WRI1. We tested the possibility of direct interaction between WRI and KIN10 and/or KIN11 using three independent methods (Figure 10). First, a bimolecular fluorescence complementation assay was employed in which the Venus N-terminal fragment and CFP C-terminal fragment were fused to KIN10 (or KIN11) and WRI1, respectively (Figure 10A). Fluorescence imaging demonstrated that both KIN10 and KIN11 associated strongly with WRI1, with the signal localized to the nucleus. No signal was observed for the $Venus^N$-MYB107 negative control (Figure 10A). Second, yeast two-hybrid analysis showed that BD-KIN10 and BD-KIN11 were able to interact with AD-WRI1 specifically; no growth was observed when AD-EV was substituted for AD-WRI1 (Figure 10B). A third approach involved immunoprecipitation following coexpression of GFP-WRI1 and KIN10 in infiltrated *N. benthamiana* leaf tissue. GFP-trap pull-downs were used to recover GFP-WRI1 from extracts that subsequently were separated by SDS-PAGE. Duplicate immunoblots were probed with anti-WRI1 or anti-KIN10 antibodies. KIN10 signal was present only in samples coexpressing GFP-WRI1 and KIN10, confirming their in vivo interaction (Figure 10C).

KIN10 Specifically Phosphorylates WRI1

The findings that KIN10 activity was required for WRI1 degradation, that phosphorylated WRI1 could be recovered from tissue extracts, and that KIN10 could directly interact with WRI1 raised the possibility that KIN10 may be capable of phosphorylating WRI1. To test this hypothesis, we employed a well-established in vitro KIN10 kinase assay (Shen et al., 2009) using

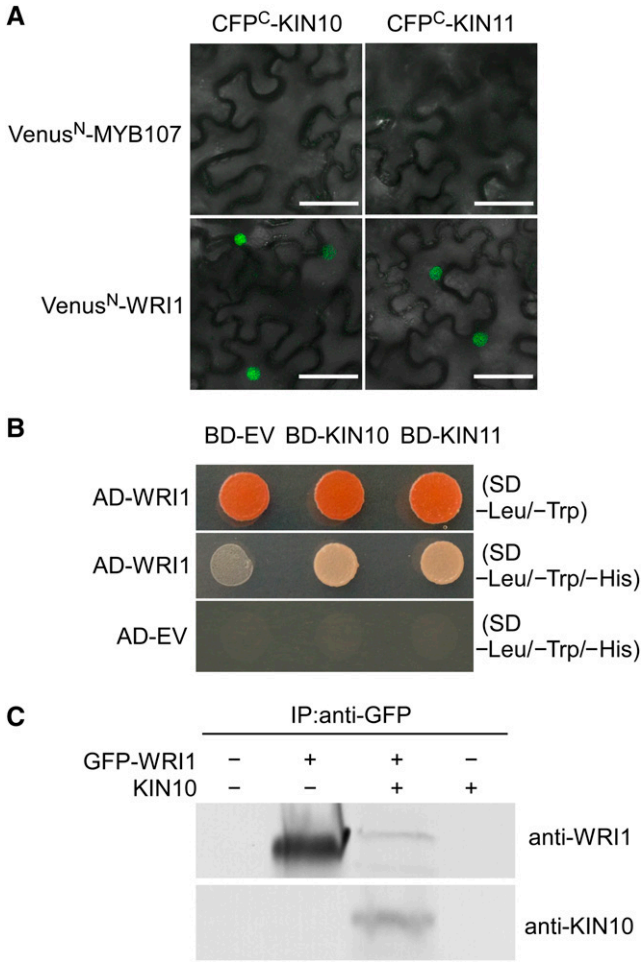

Figure 10. KIN10 and KIN11 Interact with WRI1.

(A) Visualization of WRI1 interactions with KIN10 or KIN11 interactions using a bimolecular fluorescence complementation assay in *N. benthamiana* pavement cells. Construct designations: Venus^N, N-terminal fragment of Venus protein; CFP^C, C-terminal fragment of CFP protein. Nucleus-localized MYB107 was used as a negative control.

(B) KIN10/KIN11-WRI1 interaction yeast two-hybrid analysis. SD/−Leu/−Trp medium was used for transformation selection; SD/−Leu/−Trp/−His medium was used to test for interactions. BD, binding domain; AD, activation domain; SD, synthetic defined medium.

(C) GFP-WRI1 was isolated using GFP trap (ChromoTek) from *N. benthamiana* leaves coexpressing KIN10 and GFP-WRI1 as indicated. Anti-WRI1 and anti-KIN10 antibodies were used to detect the precipitated WRI1 and KIN10 proteins respectively.

E. coli-expressed purified proteins, in which the transfer of a radiolabeled phosphate group from [γ-^{32}P]ATP to the target protein can be monitored. After incubation, the assay mixture was separated by SDS-PAGE, transferred to a PDVF membrane, and visualized by autoradiography. In addition to KIN10, WRI1, and [γ-^{32}P]ATP, the KIN10-activating protein kinase GRIK1 was also included (Shen et al., 2009). As shown in Figure 11A, the labeled phosphate group of ATP could be transferred to all three protein components, i.e., GRIK1, KIN10, and WRI1. The phosphorylation of WRI1 occurred only in the presence of both KIN10 and GRIK1, with no phosphorylation of WRI1 observed in reactions lacking either component. A similar amount of WRI1 phosphorylation was detected using either a 0.5 or a 0.1 ratio of the activating kinase GRIK1 to KIN10. The observation that no WRI1 phosphorylation was observed upon incubation of WRI1 with GRIK1 in the absence of KIN10 demonstrated that WRI1 phosphorylation was specifically dependent upon KIN10. Probing a duplicate blot with anti-WRI1 antibodies demonstrated that equal amounts of WRI1 were present in each reaction (Figure 11B).

WRI1 Is Phosphorylated by KIN10 at Ser-166

Our finding that WRI1 is a KIN10 target raised the question of the site(s) of phosphorylation. We first scanned the WRI1 sequence for the canonical KIN10 phosphorylation motif (MLVFI)X(RKH)XX(**ST**)XXX(LFIMV) in which the **S** or **T** is the residue targeted for phosphorylation (Halford et al., 2003). As shown in Figure 12, WRI1 contained two close matches to this sequence, in which only the last hydrophobic residue was substituted for another hydrophobic residue, i.e., IYRGVTRHRW and FSRGVSKYRGV. These two sites were located at the N-terminal border of each of the two AP2 repeats, the first containing a T and the second containing an S as the putative phosphorylation targets.

An aliquot of the GRIK1, KIN10, and WRI1-containing sample used for the experiments shown in Figure 11 was incubated with chymotrypsin and the resulting fragments analyzed by liquid chromatography/mass spectrometry-tandem mass spectrometry (MS/MS). The two motif fragments RGVTRHRW and SRGVSKY expected from this digestion would both be hydrophilic in nature making them difficult to analyze by this approach. However, one of the two peptides, SRGVSKY, phosphorylated at the underlined S was unambiguously identified (Figure 13). We were unable to detect the unphosphorylated form of this peptide in repeated trials, suggesting that it is highly phosphorylated. To date, we have been unsuccessful in detecting the RGVTRHRW peptide or its phosphorylated form.

Phosphorylation of WRI1 Is Inhibited in the Presence of Its Target DNA

The phosphorylation site at Ser-166 and the putative phosphorylation site at Thr-70 (diagrammed as green bars in Figure 12) overlap with the N-terminal margins of two AP2 DNA binding domains within WRI1 (shown in yellow in Figure 12). We therefore tested whether incubation of WRI1 with fragments of DNA encoding its target sites would impede phosphorylation. We performed KIN10 and GRIK1-dependent phosphorylation assays in the presence of DNA fragments containing the promoter sequences of two WRI1 target genes: *BCCP2* and *PKPβ1* (Figure 14A) (Maeo et al., 2009). WRI1 phosphorylation was observed in assays lacking DNA supplementation and in those supplemented with 35S promoter DNA. By contrast, assays containing the WRI1 target DNA fragments from *BCCP2* and *PKPβ1* showed reduced levels of phosphorylation (Figure 14A).

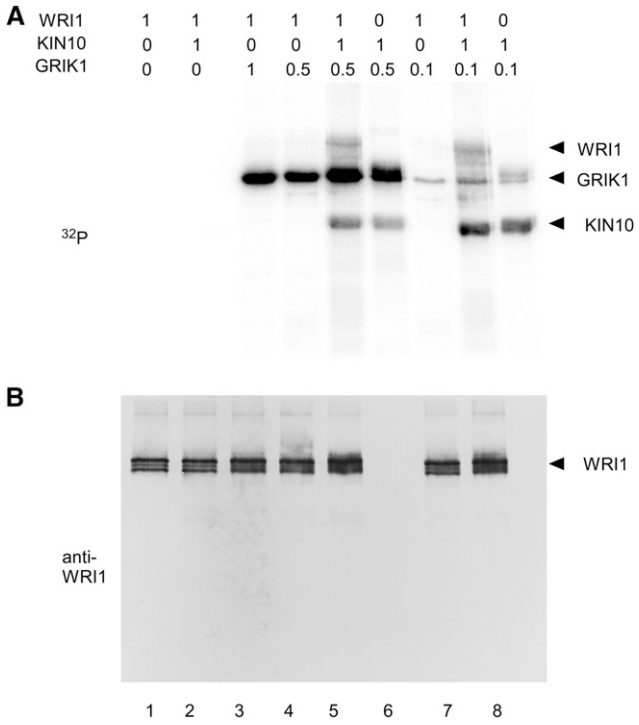

Figure 11. KIN10-Dependent Phosphorylation of WRI1.

(A) In vitro assays were performed using *E. coli*-expressed, purified WRI1, KIN10, and GRIK1 components. Reactions contained the amount of each protein (μg) indicated above the corresponding lane, in the presence of [γ-^{32}P]ATP. The assay reactions were resolved by SDS-PAGE and transferred to PVDF membranes. ^{32}P-labeled proteins were visualized by autoradiography.

(B) Anti-WRI1 antibody was used to probe the membrane visualized by autoradiography in **(A)**.

WRI1 Mutants T70A, S166A, and T70A/S166A Are Less Susceptible to KIN10-Dependent Phosphorylation and Degradation Relative to Wild-Type WRI1

To directly assess Thr-70 and Ser-166 as target sites within WRI1, three site-specific mutants, T70A, S166A, and T70A/S166A, were engineered and subjected to KIN10 kinase assay. As shown in Figure 14B, phosphorylation of the two single mutants was slightly reduced in intensity, whereas the T70A/S166A double mutant lacked detectable phosphorylation signal. These data are consistent with phosphorylation of these two sites by KIN10.

The stability of WRI1 mutants T70A, S166A and T70A/S166A were assessed relative to that of WRI1 upon co-expression with *KIN10* in *N. benthamiana*. As shown in Figure 14C, mutation of the two putative KIN10 phosphorylation sites resulted in significantly higher accumulation of WRI1 polypeptide, by 2-3 fold relative to wild-type WRI1.

Phosphorylated WRI1 Is Degraded More Rapidly Than Native WRI1

The phosphorylation of many proteins results in their degradation via the ATP-dependent ubiquitin/proteasome pathway. We have demonstrated in this research that KIN10 facilitates WRI1 degradation and that KIN10 can phosphorylate WRI1. Accordingly, we next tested whether phosphorylation of WRI1 results in rapid degradation relative to the nonphosphorylated form. We isolated either phosphorylated or unphosphorylated WRI1 by immunoprecipitation from assays containing KIN10 and GRIK1 in the presence or absence of ATP, respectively. The resulting phosphorylated WRI1 or native WRI1 samples were incubated with freshly prepared Arabidopsis leaf extracts, and samples were removed for analysis at various time points (Figure 15). The phosphorylated form of WRI1 was degraded significantly more rapidly than the unphosphorylated form.

DISCUSSION

Lipid biosynthesis is a highly carbon-, energy-, and reductant-demanding process, but little is known about coordination between the regulation of lipid biosynthesis and that of cellular energy/sugar status. Here, we identify links between these processes by studying WRI1, the master transcriptional regulator of fatty acid biosynthesis, and demonstrate its phosphorylation by KIN10, a factor that plays a major role in sugar/energy sensing and homeostasis.

These findings arose from our testing the hypothesis that *KIN10* expression should boost fatty acid biosynthesis by stabilizing the FUS3 transcription factor (Gazzarrini and Tsai, 2015), a positive regulator of WRI1 (Baud and Lepiniec, 2010). We rejected this hypothesis because KIN10-OX Arabidopsis seeds showed a reduction rather than the predicted enhancement of fatty acid/TAG accumulation and because coexpression of *WRI1/OLE1* with *KIN10* abrogated *WRI1/OLE1*'s stimulatory effects on TAG accumulation. Together, these results implied KIN10 is a negative, rather than a positive, regulator of TAG accumulation. Such a role would be consistent with KIN10's well-established role in enhancing catabolism while repressing anabolism as a homeostatic mechanism to balance cellular energy levels with metabolism (Rolland and Sheen, 2005). Because the activity of KIN10 is repressed when sugar levels are elevated (Baena-Gonzalez et al., 2007), degradation of WRI1 would be repressed, resulting in its accumulation, thereby upregulating lipid biosynthesis. This scenario identifies a specific mechanistic role for sugar in potentiating WRI1-controlled fatty acid biosynthesis beyond the supply of

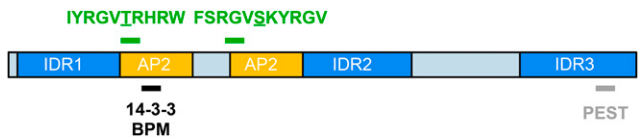

Figure 12. Schematic Diagram of the WRI1 Predicted Protein Sequence Illustrating the Locations of Known Domains.

The two AP2 DNA binding domains are shown in yellow; three intrinsically disordered regions (IDR) are shown in blue. Two KIN10 phosphorylation sites are shown as green bars. The 14-3-3 phosphopeptide binding site and BPM binding site colocalize to the same region represented by a black bar. The C-terminal PEST domain, rich in Pro, Glu, Ser, and Thr residues within IDR3, is represented as a gray bar.

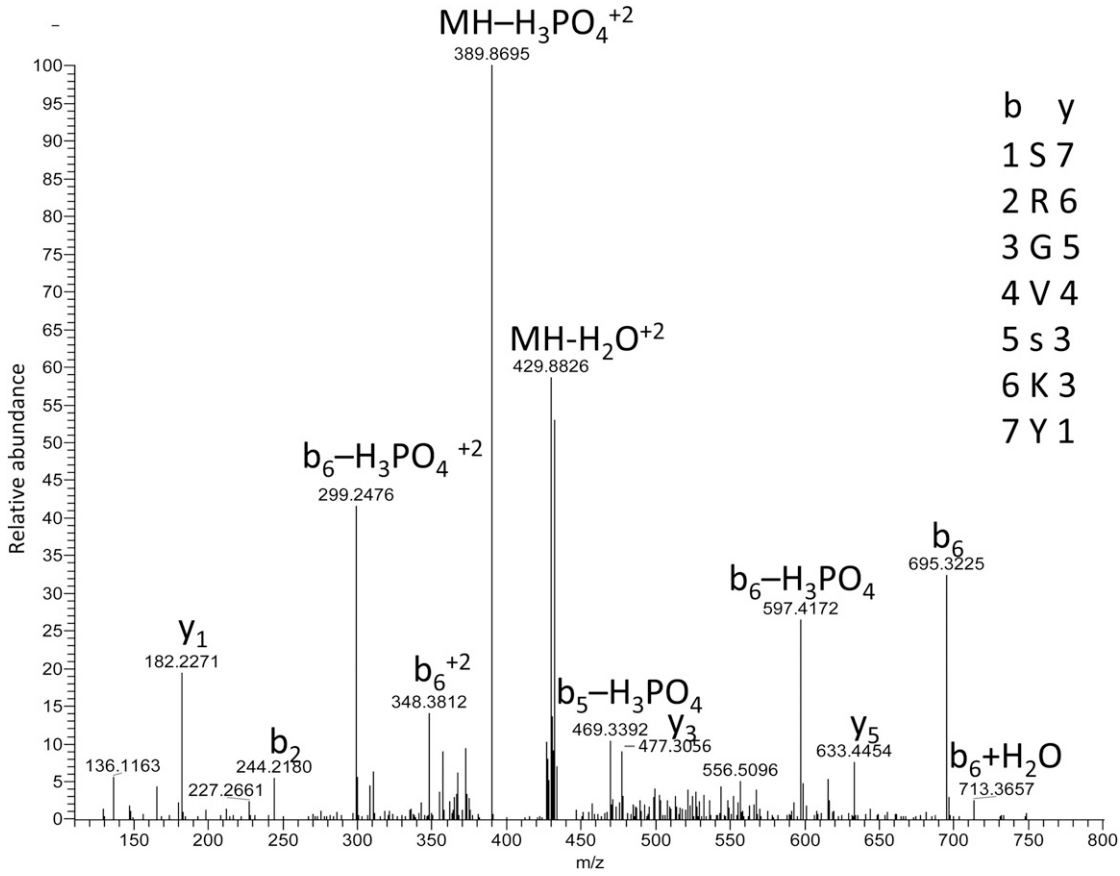

Figure 13. Annotated MS/MS Spectrum for Phosphorylated Peptide SRGVSKY Generated by Chymotrypsin Digestion of WRI1.

The doubly charged ion of this phosphorylated peptide (MH^{2+}) had a theoretical *m/z* of 438.7024 (mono) and 438.9470 (av) and the parent ion of this spectra had an *m/z* of 438.7061. The sequence of the peptide is given in the right vertical panel indicating associated y and b ions. The phosphorylated serine is indicated by the lowercase s (i.e., SRGVsKY). Evidence of phosphorylation is provided by the parent ion *m/z* and good sequence coverage with spectral lines for the y_1, b_6, y_3, b_5, y_5, and b_2 fragments.

carbon skeletons previously described to rationalize sugar potentiation of WRI1 (Cernac and Benning, 2004; Sanjaya et al., 2011) and the mild transcriptional activation of *WRI1* in the presence of very high levels of sugar (Masaki et al., 2005). Having identified the KIN10-dependent inhibition of fatty acid accumulation, we set out to understand the molecular mechanism underlying these findings.

Our contention that KIN10-dependent phosphorylation of WRI1 results in its degradation via a proteasomal pathway resulting in a downregulation of lipid biosynthesis is consistent with the following observations: (1) Overexpression of *KIN10* results in reduced levels of WRI1 polypeptide, but not *WRI1* mRNA, in both *N. benthamiana* leaves and Arabidopsis siliques. (2) Coexpression of KIN10 mutants with reduced phosphorylation activity result in lower levels of WRI1 degradation. (3) Phosphorylated forms of WRI1 can be detected in extracts of *N. benthamiana* and *B. napus*. (4) Infiltration of the potent proteasome inhibitor bortezomib into *N. benthamiana* leaves expressing *WRI1* either alone or with *KIN10* resulted in increased accumulation of WRI1 relative to controls lacking the inhibitor. (5) Reduced levels of WRI1 in developing seeds correlated with significantly reduced expression of WRI1-target genes and significantly decreased levels of TAG accumulation.

That KIN10 directly phosphorylates WRI1 rather than via an indirect cascade mediated by one of its many hundreds of targets is supported by evidence of their direct interaction in bimolecular fluorescence complementation, yeast two-hybrid assays, and coimmunoprecipitation assays. Furthermore, in vitro assays using *E. coli*-expressed purified components show that WRI1 phosphorylation is dependent upon the presence of both KIN10 and its activator, GRIK1. That WRI1 lacks a canonical KIN10 target sequence raised the question as to the identity of the phosphorylation site(s). Manual inspection of the WRI1 sequence led the identification of Thr-70 and Ser-166 as putative targets because they are located within close variants of the canonical KIN10 target sequence in the first and second AP2 DNA binding domains, respectively. That these residues are bona fide targets of KIN10 phosphorylation is supported by (1) decreased phosphorylation of WRI1 in the presence of WRI1 target promoter fragments, with inhibition greater for *BCCP2* than for *PKPβ1*, consistent with their

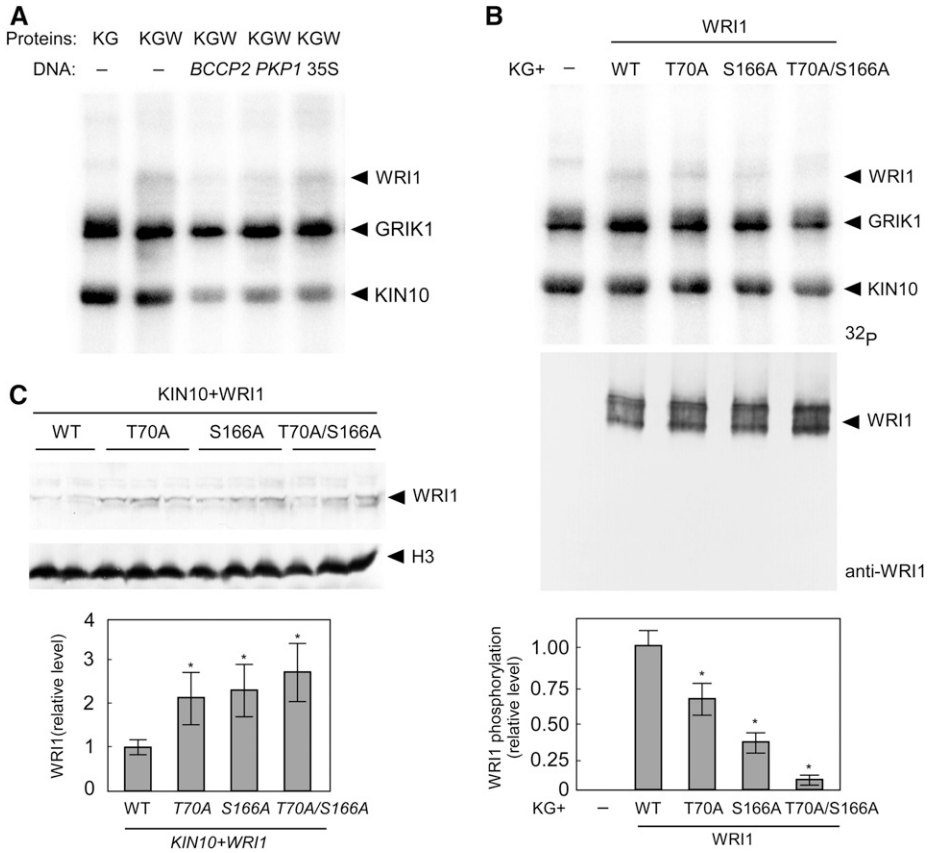

Figure 14. Localization of KIN10-Dependent WRI1 Phosphorylation Sites to Thr-70 and Ser-166 in Its AP2 DNA Binding Domains.

(A) Autoradiogram of KIN10-dependent WRI1 kinase assays performed as described in the Figure 11 legend. Promoter fragments of two WRI1 target genes, *BCCP2* and *PKPβ1*, along with the negative control 35S promoter were used to supplement the assays as indicated. K, KIN10; G, GRIK1; W, WRI1.
(B) Top: KIN10-dependent WRI1 kinase assays using WRI1 variants containing mutations at two putative KIN10 phosphorylation sites, T70A and S166A, along with the double mutant T70A/S166A. Middle: Anti-WRI1 antibody immunoblot to visualize the WRI1 load. Bottom: Quantification of signal of WRI1 phosphorylation. Significant differences are indicated compared with wild-type WRI1 ($n = 3$, ±SD; Student's t test, *$P < 0.05$).
(C) Anti-WRI1 immunoblot of extracts from *N. benthamiana* leaves expressing *WRI1* and mutants *T70A*, *S166A*, and *T70A,S166A* cotransformed with *KIN10*. Antihistone H3 antibody was used to probe a duplicate immunoblot as a loading control. The histogram below the blot shows the quantification of signal from WRI1 ($n = 3$, ±SD), and significant differences are indicated compared with wild-type WRI1 (Student's t test, *$P < 0.05$).

relative levels of activation by WRI1 (Maeo et al., 2009); (2) the absence of detectable phosphorylation of the WRI1 T70A/S166A double mutant but presence of phosphorylation in each of the Thr-70 and Ser-166 single mutants from in vitro assays; and (3) the direct detection of a chymotriptic fragment corresponding to phosphorylated SRGVSKY, with a fragmentation pattern diagnostic for phosphorylation at Ser-166. The hypothesis that KIN10 phosphorylation of WRI1 is related to its degradation is supported by the observed increase in accumulation of WRI1 polypeptide upon expression of the individual phosphorylation site mutants T70A and S166A or the T70A/S166 double mutant relative to wild-type WRI1 when coexpressed with KIN10. In addition, the rapid degradation of in vitro KIN10-phosphorylated WRI1 relative to native WRI1 in cell-free degradation assays is consistent with this view.

One observation that we do not yet fully understand is the nature of the ensemble of apparent molecular masses of WRI1 that accumulate naturally in Arabidopsis seeds and upon inducible expression in Arabidopsis leaves. One possible explanation is that other, not yet identified posttranslational modifications of WRI1 contribute to this heterogeneity. As shown in Supplemental Figure 5, glycosylase treatment did not substantially affect the distribution of WR1-immunoreactive molecular species, suggesting that glycosylation is not a major contributor to the observed heterogeneity. However, our observation that phosphorylation leads to proteasomal degradation is consistent with the identification of a fraction of the WRI1 being conjugated to ubiquitin. Once conjugated to WRI1, the ubiquitin could itself become ubiquitinated to form ubiquitin ladders of varying lengths that contribute to a heterogeneous ensemble such as that observed in this study. This scenario is appealing in that ubiquitin conjugation targets proteins for degradation via the proteasome. Our identification of a dilysine motif at the N terminus of WRI1, that when mutated to arginine residues results in increased accumulation of

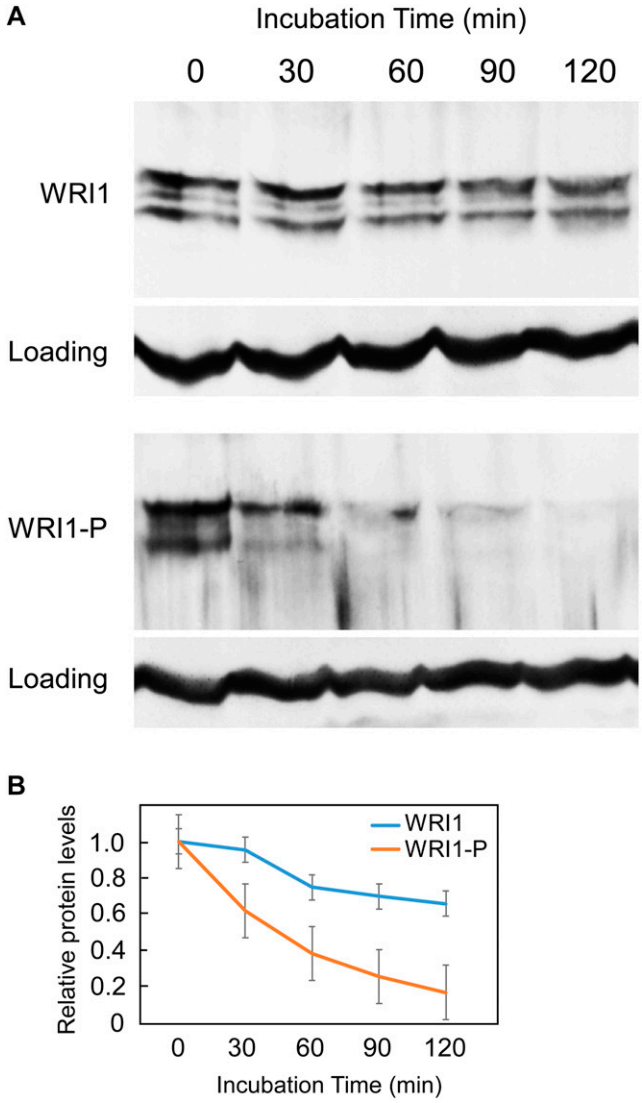

Figure 15. Phosphorylated WRI1 Is Degraded Faster Than Native WRI1 in a Cell-Free Degradation Assay.

(A) Samples of phosphorylated WRI1 or nonphosphorylated WRI1 were collected by immunoprecipitation from in vitro kinase reactions containing WRI1, KIN10, and GRIK1 supplemented with ATP or lacking ATP, respectively. Equal amounts of phosphorylated or nonphosphorylated WRI1 preparations were incubated with freshly prepared Arabidopsis crude leaf extract supplemented with ATP for time as indicated (in minutes).

(B) Quantitation of WRI1 and WRI1-P immunoblot signals during cell degradation assays. Values represent mean ± SD of immunoblot signals from three independent experiments.

WRI1, provides a connection between possible ubiquitin target residues and the stability of WRI1. Such a hypothesis is consistent with reports that the C-terminal KEKE sequence of the α-4/PAD1 subunit of the 20S proteasome binds KIN10 along with SKP1/ASK1 (Farrás et al., 2001). Based on this, it is tempting to speculate that the proteasome-KIN10 complex recruits WRI1, phosphorylates it, and under the Skip, Cullin F-box (SCF) paradigm (Bai et al., 1996; Skowyra et al., 1997) ubiquitilates the phosphorylated WRI1 that is subsequently degraded by the proteasome to which the KIN10-SCF complex is tethered. Further work will be required to test details of this model.

Several previous reports have described proteasomal degradation of WRI1 (Chen et al., 2013; Ma et al., 2015, 2016). One involves a PEST sequence representing a potential phosphorylation site identified in the C-terminal intrinsically disordered region of WRI1 (IDR3-PEST; Figure 11) (Ma et al., 2015). Deletion of the PEST domain increased the stability of a bacterially expressed fusion protein relative to full-length WRI1 in a cell-free protein degradation assay (Ma et al., 2015). However, the KIN10 target residues identified herein are distant from the PEST domain, indicating that the mechanisms are distinct. A second report by the same group demonstrated that 14-3-3 phosphopeptide binding proteins bind to and stabilize WRI1, leading to increased TAG accumulation (Ma et al., 2016). The 14-3-3 binding site was mapped to WRI1 residues 78 to 92, the same region that interacts with the BPM proteins that act as substrate adaptors to a CULLIN3-based E3 ligase (Chen et al., 2013) (Figure 12), leading the authors to hypothesize that 14-3-3 proteins compete with E3-adapter binding, thereby stabilizing WRI1 (Ma et al., 2016). This 14-3-3/BPM1 binding region is immediately adjacent to the KIN10 phosphorylation site (residues 65−74) in the first AP2 domain of WRI1 (Figure 12), suggesting potential overlap between the two described phenomena, possibly involving the ubiquitin-proteasomal degradation pathway. 14-3-3 proteins have also been reported to bind to phosphorylated forms of enzymes such as nitrate reductase causing their inactivation (Moorhead et al., 1996).

In this work, we identified two cryptic KIN10 target sites with physiological relevance to WRI1 degradation, but note that an SnRK2.6 (OST1) phosphorylation target sequence (LRRQSSGFSR) was previously identified in residues 154 to 163 (Sirichandra et al., 2010), suggesting the possibility of additional phosphorylation-dependent regulation of WRI1.

An apparent paradox when we initiated this work was that KIN10-RNAi and KIN10-OX both result in a decrease in seed oil. A potential explanation is that KIN10 plays independent regulatory roles in several processes including the degradation of WRI1 in addition to activating α-amylase (Laurie et al., 2003; Baena-González et al., 2007; Hedbacker and Carlson, 2008). Rice (*Oryza sativa*) seed containing a mutant ortholog of KIN10/KIN11 accumulates more starch and less lipid than wild-type seed (Fu et al., 2009). Similarly, the starch content analyzed herein increased from ~5% in wild-type seeds to 10% in KIN10-RNAi seeds. Thus, compromised flow of carbon from starch to fatty acid biosynthesis provides a possible explanation for the observed reduced TAG phenotype in KIN10-RNAi seeds.

Because sugar homeostasis/signaling is a conserved metabolic imperative across the kingdoms of life, we searched the literature for connections between sugar signaling and lipid metabolism in other systems. In mammals, protein phosphorylation is reported to play an important role in the regulation of lipid biosynthesis. Insulin, a major regulator of blood glucose, regulates de novo lipogenesis via sterol regulatory element binding proteins (SREBPs) that play an analogous role to that of WRI1 in plants. SREBPs control the expression of genes required for production of cholesterol, fatty acids, triglycerides, and phospholipids

(Ferré and Foufelle, 2007). Metformin, a drug commonly used to treat diabetes, potentiates AMP-activated protein kinase (Zhou et al., 2001), which directly phosphorylates and inhibits SREBP activity (Li et al., 2011). This raises the possibility that phosphorylation of WRI1 within each of its two DNA binding domains could both target WRI1 for degradation and cause its inactivation. Conversely, phosphorylation of WRI1 could both stimulate its transcriptional activity and increase its degradation, thereby facilitating tight control of lipid biosynthesis. The latter scenario is consistent with the reported stabilization of WRI1 by the 14-3-3 phosphopeptide binding protein (Ma et al., 2016).

In summary, the evidence presented here shows that KIN10 negatively regulates WRI1 protein levels by phosphorylating it at two previously unidentified KIN10 target sites, each associated with one of the two AP2 DNA binding domains of WRI1. Site-specific mutagenesis of Thr-70 and Ser-166 to Ala stabilized WRI1 when coexpressed with KIN10. The KIN10-dependent degradation was shown to be proteasomal as evidenced by its inhibitor sensitivity. While it is presently unknown whether WRI1 degradation proceeds via the ubiquitin pathway, the close association within the WRI1 sequence of the BPM1 substrate adapter binding domain of the CULLIN3-based E3 ligase to that of the Thr-70 KIN10 phosphorylation site in addition to the previously described interactions of KIN10 with the proteasomal subunit α-4/PAD1 and SKP1/ASK1 (Farrás et al., 2001) complex provide two possible links to the ubiquitin-dependent proteasomal degradation pathway (Hua and Vierstra, 2011). That KIN10-dependent phosphorylation of WRI1 leads to its degradation provides a mechanistic link between a critical effector of energy/sugar homeostasis and that of a major regulator of lipid biosynthesis. Knowledge of the details of this regulatory circuit may be of use in designing strategies to increase TAG accumulation for biotechnological applications.

METHODS

Plant Materials and Growth Conditions

KIN10-OX and RNAi *KIN10*-suppressed *Arabidopsis thaliana* lines were obtained from Jen Sheen (Baena-González et al., 2007). Arabidopsis seeds were surface-sterilized and selected on agar plates containing half-strength Murashige and Skoog salts. After 1 week, seedlings were transplanted to moist PM-15-13 AIS MIX (Lehle Seeds). All plants (Arabidopsis and tobacco [*Nicotiana benthamiana*]) were grown with a 16-h-light/8-h-dark photoperiod (combination of cool white fluorescent lamps and incandescent lamps, at a photosynthetic photon flux density of 250 μmol m^{-2} s^{-1}) at a 23°C/19°C light/dark temperature regime and ~75% relative humidity. For induction of expression for ethanol-inducible gene, roots of transgenic plant lines were irrigated with 2% ethanol.

Genetic Constructs

OLE1, *WRI1*, *WRI1^{RR}* *KIN10*, and *KIN11* were amplified by PCR from genomic DNA or Arabidopsis seed cDNA using primer pairs listed in Supplemental Table 1. The PCR products were cloned into Gateway pDONR/Zeo Vector (Invitrogen) by BP reaction and by LR reaction subcloned into plant Gateway binary vectors pGWB414 (Nakagawa et al., 2007), pMDC85 (ABRC), pMDC43(ABRC), pDEST-VYNE(R) GW, and pDEST-SCYCE (R) GW (Gehl et al., 2009) or yeast two-hybrid expression vectors pDEST-GADT7 and pDEST-GBKT7 (Invitrogen). *WRI1* coding sequence (CDS) was also amplified by PCR and inserted between *Xho*I and *Bam*HI of vector pET15b (Novagen) for production of recombinant WRI1 protein in *Escherichia coli* BL21(DE3). The *GRIK1* CDS was removed with *Eco*RI and *Xho*I from vector pGEX-5X-3 (pNSB1554; Shen et al., 2009) and inserted between the *Eco*RI and *Xho*I sites of pET28b (Novagen) for production of recombinant His-tag GRIK1. CDSs of *KIN10* mutants T175A and K48M (Crozet et al., 2016) were amplified by PCR and cloned into pGWB414 for tobacco transient expression assays. *WRI1* mutants *WRI1(T70A)*, *WRI1(S166A)*, and *WRI1(T70A/S166A)* were constructed using primers pairs listed in Supplemental Table 1 and cloned into both pGWB414 and pET15 for expression in *E. coli* and plants, respectively. *KIN10(T175A)* and *KIN10(K48M)* were obtained from Elena Baena-González (Crozet et al., 2016).

Agroinfiltration of *N. benthamiana* and Protein Extraction

Transient gene expression in *N. benthamiana* by agroinfiltration was accomplished using a previously described procedure (Ohad and Yalovsky, 2010). Infiltrated leaves were harvested 3 d after inoculation with different gene combinations and analyzed for or protein content and/or TAG accumulation. For examining protein accumulation, ~50 mg leaf discs were transferred to Eppendorf tubes, frozen under liquid N_2, and ground to a powder. SDS sample buffer (150 μL) at 95°C was added to the frozen powder and mixed using a vortex mixer. The slurry was incubated for 5 min at 95°C and cleared by centrifugation before loading for PAGE analysis. For bortezomib treatment, *N. benthamiana* leaves were infiltrated with WRI1 +EV or WRI1+KIN10 for 3 d. On day 4, those infiltrated leaves were again infiltrated with buffer only or buffer containing 0.1 μM bortezomib for another 12 h.

Antibodies and Immunoblotting

Anti-WRI1, -KIN10, -ubiquitin, and -Histone H3 antibodies were used in this study. Anti-WRI1 polyclonal antibodies were raised in rabbits immunized with a synthetic peptide (DFMFDDGKHECLNLENLDC) corresponding to residues 299 to 317 of the WRI1 amino acid sequence (Pierce, Thermo Fisher). Anti-KIN10, -ubiquitin, and -Histone H3 polyclonal antibodies were purchased from Agrisera (catalog nos. AS10919, AS10307S, and AS10710). For each antibody, 1:1000 dilution was used. Proteins were resolved by SDS-PAGE and transferred to PVDF membrane for immunoblot analysis. Immunoblots of targeted proteins were visualized using alkaline phosphatase-conjugated secondary antibodies and 5-bromo-4-chloro-3-indolylphosphate/nitro-blue tetrazolium substrate (Bio-Rad).

Expression and Purification of Recombinant WRI1, KIN10, and GRIK1

Recombinant WRI1, KIN10, and GRIK1 proteins with N-terminal His-tag were expressed in *E. coli* BL21(DE3). Protein purification was performed as reported by Nallamsetty (Nallamsetty and Waugh, 2007). Briefly, 1 liter of LB was inoculated with 10 mL of a saturated growth *E. coli* culture and incubated at 37°C with shaking at 225 rpm until its optical density A_{600} reached 0.6, at which time the temperature of the culture was reduced to 16°C for 30 min before the addition of isopropyl β-D-1-thiogalactopyranoside to a final concentration of 0.4 mM. The culture was incubated for a further 16 h. Cells were collected by centrifugation at 6000*g* for 15 min and resuspended in a lysis buffer containing 20 mM Tris-HCl (pH 8.0), 0.5 M NaCl, and 0.1% Triton X-100. The cells were disrupted by passage through a French pressure cell (SLM Aminico) at 10,000 p.s.i. The cell lysate was clarified by centrifugation at 15,000*g* for 30 min at 4°C. The supernatant was applied to a Ni-NTA resin column equilibrated in lysis buffer supplemented with 25 mM imidazole (loading buffer). The column was washed with loading buffer until a stable baseline was obtained, and the bound

proteins were eluted with 20 mM Tris-HCl (pH 8.0), 0.5 M NaCl, and 10% glycerol supplemented with 500 mM imidazole. The eluted protein samples were desalted using an Econo-Pac 10DG chromatography column (Bio-Rad) into 20 mM Tris-HCl (pH8.0), 0.5 M NaCl, 50% glycerol, and 1 mM DTT. Protein preparations were and stored at −20°C until use.

TAG and Total Fatty Acid Quantification

Total lipids (TAG plus polar lipids) were isolated from 100 mg of freshly harvested leaf tissue by the addition of 700 μL of methanol:chloroform: formic acid (2:1:0.1, v/v/v) by vigorous shaking for 30 min, after which 1 mL of 1 M KCl and 0.2 M H_3PO_4 was added. After mixing, the samples were centrifuged at 1500*g*, and total lipids were collected. For TAG quantification, 60 μL of total lipid was separated by Silica Gel 60 (Merck) TLC developed with hexane:diethyl ether:acetic acid (70:30:1, v/v/v) and visualized by spraying with 0.05% primuline (in 80% acetone). TAG fractions identified under UV light were isolated from the plate and transmethylated to fatty acid methyl esters by incubation in 1 mL boron trichloride-methanol at 85°C for 40 min. For total fatty acid quantification, 10 μL of total lipids was directly transmethylated with boron trichloride-methanol as described above. For both assays, 5 μg C17:0 was added as internal standard prior to transmethylation. Fatty acid methyl esters were extracted into hexane and dried under a nitrogen stream before being dissolved in 100 μL hexane and analyzed by gas chromatography-mass spectrometry with an Agilent Technologies 7890A GC system equipped with an Agilent 60m DB23 capillary column (i.d. 250 μm) and a 5975C mass selective detector.

In Vivo [1-^{14}C] Acetate Labeling

Labeling experiments were performed essentially as described by Koo et al. (2004). *N. benthamiana* leaves were incubated in 25 mM MES (pH 5.7) buffer containing 0.01% w/v Tween 20 as wetting agent under illumination (180 μmol m^{-2} s^{-1}) at 25°C. Labeling was initiated by the addition of 10 μCi of sodium [1-^{14}C] acetate solution (58 mCi/mmol; American Radiolabeled Chemicals). Labeling was terminated by removal of the medium from the leaf, and the sample was washed three times with water. Total lipids were extracted and separated as described above. Radioactivity associated with total lipids was determined by liquid scintillation counting using a Tricarb (Perkin-Elmer).

Starch Quantification

Starch in developing seeds was quantified using a Starch (HK) Assay Kit (Sigma-Aldrich) according to the manufacturer's protocol.

RNA Isolation and RT-qPCR

To quantify gene expression in transgenic plants or agroinfiltrated *N. benthamiana* leaves, total RNAs were extracted using an RNeasy Plant Mini Kit (Qiagen) following the manufacturer's instructions. cDNA was prepared using SuperScript III First-Strand Synthesis SuperMix (Invitrogen). qPCR was performed using the CFX96 qPCR detection system (Bio-Rad) and gene-specific primers for *WRI1*, *KIN10*, *BCCP2*, *KAS1*, and *PKPβ1*, with *F-box* (At5g15710 for Arabidopsis; Niben.v0.3.Ctg24993647 for *N. benthamiana*) as a reference gene, using oligonucleotide primers as described in Supplemental Table 1. Statistical analysis of RT-qPCR data was performed using the REST2009 algorithm (Pfaffl et al., 2002).

Protein Interaction Analysis by Yeast Two-Hybrid, Bimolecular Fluorescence Complementation, and Coimmunoprecipitation

Yeast two-hybrid assay was performed as described in the Clontech Yeast Protocols Handbook. The bimolecular fluorescence complementation assay was performed as described by Gehl et al. (2009). Fluorescence from the combined Venus N- and CFP C-fragments was imaged using a Leica SP5 confocal laser scanning microscope using an excitation wavelength of 515 nm (GFP-WRI1 is imaged with the same setting). Coimmunoprecipitation of protein complex from infiltrated *N. benthamiana* leaves was performed as described previously (Ohad and Yalovsky, 2010). Briefly, coinfiltrated tobacco leaves were ground in liquid nitrogen, homogenized in NEB buffer (20 mM HEPES, pH 7.5, 40 mM KCl, 1% Triton X-100, and protein inhibitor cocktail), and clarified by centrifugation at 16,000*g* for 15 min. Supernatant (1 mL) was mixed with 20 μL GFP-Trap bead slurry and constantly mixed for 30 min at 4°C. The beads were recovered by centrifugation at 2000*g* for 1 min and washed five times with a buffer containing 20 mM HEPES, 40 mM KCl, pH 7.5, supplemented with Triton X-100 to 0.1%. The bound proteins were eluted with 2× SDS-PAGE sample buffer and analyzed by immunoblotting.

Immunoprecipitation

WRI1 immunoprecipitation was performed with a Protein G Immunoprecipitation Kit (Sigma-Aldrich) according to the supplier's instructions. Phosphate affinity SDS-PAGE was performed using Acrylamide-pendant phos-tag, and the protein dephosphorylation reactions were performed according to the instructions of the Acrylamide-pendant Phos-tag kit obtained from Woko Chemicals.

Protein deglycosylation was performed with Protein Deglycosylation Mix (Promega) according to the supplier's protocol.

Protein Kinase Assay

The in vitro WRI1 kinase assay was performed according to Shen et al. (2009). Briefly, a 50 μL assay was performed with ~250 nM kinase and 250 nM substrate in 25 mM Tris-HCl (pH 7.5), 10 mM $MgCl_2$, 1 mM EGTA, 0.2 mM ATP, and 0.1 μCi/μL [γ-^{32}P]ATP (Perkin-Elmer) at 30°C for various times, as indicated. The reaction was terminated by addition of an equal volume of 2× SDS-PAGE loading buffer. A 20-μL aliquot of each assay was resolved by SDS-PAGE and transferred to PVDF membrane. ^{32}P-labeled proteins were visualized by autoradiography employing a phosphor screen that was analyzed by a Typhoon FLA 7000 imager (GE Healthcare). For kinase assay supplemented with WRI1 target gene promoter fragments, *BCCP2* and *PKPβ1*, 1 μg plasmid DNA containing ~1 kb of the promoter region of each gene was added to kinase reactions.

Mass Spectrometry and Data Analysis

Purified WRI1 and reaction proteins in 25 mM Tris-HCl (pH7.5), 10 mM $MgCl_2$, 1 mM EGTA, and 0.2 mM ATP were reduced by supplementation of DTT to 4 mM and alkylated in 8.4 mM iodoacetamide. The proteins were subsequently digested with chymotrypsin (Roche Diagnostics) at a 25:1 protein:chymotrypsin mass ratio, incubated 16 h at 24°C. The digests were brought to 2% formic acid and desalted with Supel-Tips C18 Micropipette Tips (Sigma-Aldrich) using formic acid-containing solutions with varied acetonitrile (ACN) as described in the manufacturer's instructions. More hydrophilic peptides were extracted from the C18 desalting flow through using Glygen TopTip graphite columns (Glygen) according to the manufacturer's instructions. The combined C18 and graphite eluates were evaporated to dryness in a vacuum centrifuge and dissolved in 2% ACN and 0.1% formic acid (buffer A) for analysis by automated microcapillary liquid chromatography-tandem mass spectrometry. Fused-silica capillaries (100 μm i.d.) were pulled using a P-2000 CO_2 laser puller (Sutter Instruments) to a 5-μm i.d. tip and packed with 10 cm of 5 μm ProntoSil 120-5-C18H (Bischoff Chromatography) using a pressure bomb. The column was installed in line with a Dionex Ultimate 3000 autosampler and HPLC system. The samples were loaded via the autosampler and eluted with the

HPLC pump running at 300 nL min^{-1}. The peptides were eluted from the column by applying a 35 min gradient from 0% buffer B (98% ACN and 0.1% formic acid) to 45% buffer B. The gradient was switched from 45 to 80% buffer B over 10 min and then changed from 80% buffer B to 0% buffer B over 10 min and held constant at 100% buffer A for 20 more minutes. The application of a 2.2-kV distal voltage electrosprayed the eluting peptides directly into an LTQ Orbitrap XL ion trap mass spectrometer (Thermo Fisher) equipped with a nano-liquid chromatography electrospray ionization source. Full mass spectra were recorded on the peptides over a 380 to 2000 *m/z* range at 60,000 resolution, followed by top-five MS/MS scans in the ion trap. Charge state-dependent screening was turned on, and peptides with a charge state of +2 or higher were analyzed. Mass spectrometer scan functions and HPLC solvent gradients were controlled by the Xcalibur data system (Thermo Fisher). MS/MS spectra were extracted from the RAW file with ReAdW.exe (http://sourceforge.net/projects/sashimi). The resulting mzXML data files were searched with Inspect (Tanner et al., 2005) against a custom database composed of the Uniprot EColi_K12 proteome with added sequences for WRI1, WRI1(C), GRIK1, KIN10, and common contaminants. The data were also analyzed using the GPM XTamden and MaXQuant Andromeda search engines.

WRI1 Cell-Free Degradation Assay

For comparing the degradation of phosphorylated WRI1 and nonphosphorylated WRI1, phosphorylated or nonphosphorylated WRI1 was collected by immunoprecipitation from in vitro kinase reactions comprising WRI1 (1 μg), KIN10 (1 μg), and GRIK1 (0.5 μg) either supplemented with or lacking ATP. Prior to immunoprecipitation, WRI1 antibody was cross-linked to protein G beads following the protocol described by Abcam. After immunoprecipitation, proteins were eluted from beads with 1 M glycine, pH 2.5, desalted into 50 mM Tris-HCl buffer, pH 7.5, and mixed with crude proteins that were extracted from 4-week-old Arabidopsis leaves in 50 mM Tris-HCl buffer, pH 7.5, containing 100 mM NaCl, 10 mM $MgCl_2$, and 5 mM DTT supplemented with 5 mM ATP at the start of the assay. Specifically, 1 μg WRI1 was incubated with 200 μL crude protein extract. At various times, 25 μL aliquots were withdrawn and mixed with an equal volume of 65°C 2× sample buffer and incubated at 65°C for 2 min before SDS-PAGE separation followed by transfer to PDVF membrane and analysis by immunoblotting.

Accession Numbers

Sequence data from this article can be found in The Arabidopsis Information Resource or GenBank database under the following accession numbers: *OLE1* (AT4G25140), *WRI1* (AT3G54320), *KIN10* (AT3G01090), *KIN11* (AT3G29160), *NbF-box* (Ctg24993647), *BCCP2* (At5G15530), *KAS1* (AT5G46290), and *PKPβ1*(AT5G52920).

Supplemental Data

Supplemental Figure 1. RT-qPCR showing the gene expression levels of *WRI1*, *KIN10*, *KIN11*, and *OLE1* relative to the *N. benthamiana* F-box gene.

Supplemental Figure 2. Nuclear localization of WRI1.

Supplemental Figure 3. Specificity of anti-WRI1 antibodies.

Supplemental Figure 4. Conserved K at N terminus of WRI1.

Supplemental Figure 5. WRI1 is not glycosylated in developing seeds.

Supplemental Table 1. Oligonucleotide primer sequence pairs used in this study.

Supplemental File 1. Statistical analysis results for each figure.

ACKNOWLEDGMENTS

This work was supported by the U.S. Department of Energy, Office of Science, Office of Basic Energy Sciences under contract number DE-SC0012704, specifically through the Physical Biosciences program of the Chemical Sciences, Geosciences, and Biosciences Division. We thank Jen Sheen (Massachusetts General Hospital, Boston) for providing the Arabidopsis KIN10 OX and RNAi transgenic plant lines, Elena Baena-González (Instituto Gulbenkian de Ciênci, Lisbon) for providing KIN10 mutants, and Wei Shen (North Carolina State University) for providing GRIK1 and KIN10. We thank Dwight Martin (State University of New York, Stony Brook) for assistance with protein mass spectrometry. We thank Rick Vierstra for sending antiubiquitin antibody. We thank Mingyue Gou for providing cDNA of MYB107. We also thank C.J. Liu, Carl Andre, and F.W. Studier for helpful discussion.

AUTHOR CONTRIBUTIONS

J.S. and Z.Z. conceived the study, analyzed and interpreted the data, and wrote the manuscript. Z.Z. and H.L. developed methods and performed experiments.

Received January 9, 2017; revised February 26, 2017; accepted March 16, 2017; published March 17, 2017.

REFERENCES

Alderson, A., Sabelli, P.A., Dickinson, J.R., Cole, D., Richardson, M., Kreis, M., Shewry, P.R., and Halford, N.G. (1991). Complementation of snf1, a mutation affecting global regulation of carbon metabolism in yeast, by a plant protein kinase cDNA. Proc. Natl. Acad. Sci. USA **88:** 8602–8605.

Alves, V.S., Pimenta, D.C., Sattlegger, E., and Castilho, B.A. (2004). Biophysical characterization of Gir2, a highly acidic protein of *Saccharomyces cerevisiae* with anomalous electrophoretic behavior. Biochem. Biophys. Res. Commun. **314:** 229–234.

Andre, C., Haslam, R.P., and Shanklin, J. (2012). Feedback regulation of plastidic acetyl-CoA carboxylase by 18:1-acyl carrier protein in *Brassica napus*. Proc. Natl. Acad. Sci. USA **109:** 10107–10112.

Baena-González, E., and Sheen, J. (2008). Convergent energy and stress signaling. Trends Plant Sci. **13:** 474–482.

Baena-González, E., Rolland, F., Thevelein, J.M., and Sheen, J. (2007). A central integrator of transcription networks in plant stress and energy signalling. Nature **448:** 938–942.

Bai, C., Sen, P., Hofmann, K., Ma, L., Goebl, M., Harper, J.W., and Elledge, S.J. (1996). SKP1 connects cell cycle regulators to the ubiquitin proteolysis machinery through a novel motif, the F-box. Cell **86:** 263–274.

Baud, S., and Lepiniec, L. (2010). Physiological and developmental regulation of seed oil production. Prog. Lipid Res. **49:** 235–249.

Baud, S., Mendoza, M.S., To, A., Harscoët, E., Lepiniec, L., and Dubreucq, B. (2007). WRINKLED1 specifies the regulatory action of LEAFY COTYLEDON2 towards fatty acid metabolism during seed maturation in Arabidopsis. Plant J. **50:** 825–838.

Celenza, J.L., and Carlson, M. (1986). A yeast gene that is essential for release from glucose repression encodes a protein kinase. Science **233:** 1175–1180.

Cernac, A., and Benning, C. (2004). WRINKLED1 encodes an AP2/EREB domain protein involved in the control of storage compound biosynthesis in Arabidopsis. Plant J. **40:** 575–585.

Chen, L., Lee, J.H., Weber, H., Tohge, T., Witt, S., Roje, S., Fernie, A.R., and Hellmann, H. (2013). Arabidopsis BPM proteins function as substrate adaptors to a cullin3-based E3 ligase to affect fatty acid metabolism in plants. Plant Cell **25:** 2253–2264.

Crozet, P., Margalha, L., Butowt, R., Fernandes, N., Elias, C.A., Orosa, B., Tomanov, K., Teige, M., Bachmair, A., Sadanandom, A., and Baena-González, E. (2016). SUMOylation represses SnRK1 signaling in Arabidopsis. Plant J. **85:** 120–133.

Farrás, R., Ferrando, A., Jásik, J., Kleinow, T., Okrész, L., Tiburcio, A., Salchert, K., del Pozo, C., Schell, J., and Koncz, C. (2001). SKP1-SnRK protein kinase interactions mediate proteasomal binding of a plant SCF ubiquitin ligase. EMBO J. **20:** 2742–2756.

Ferré, P., and Foufelle, F. (2007). SREBP-1c transcription factor and lipid homeostasis: clinical perspective. Horm. Res. **68:** 72–82.

Focks, N., and Benning, C. (1998). wrinkled1: A novel, low-seed-oil mutant of Arabidopsis with a deficiency in the seed-specific regulation of carbohydrate metabolism. Plant Physiol. **118:** 91–101.

Fu, F.-F., Ye, R., Xu, S.-P., and Xue, H.-W. (2009). Studies on rice seed quality through analysis of a large-scale T-DNA insertion population. Cell Res. **19:** 380–391.

Gazzarrini, S., and Tsai, A.Y. (2015). Hormone cross-talk during seed germination. Essays Biochem. **58:** 151–164.

Gehl, C., Waadt, R., Kudla, J., Mendel, R.-R., and Hänsch, R. (2009). New GATEWAY vectors for high throughput analyses of protein-protein interactions by bimolecular fluorescence complementation. Mol. Plant **2:** 1051–1058.

Graceffa, P., Jancsó, A., and Mabuchi, K. (1992). Modification of acidic residues normalizes sodium dodecyl sulfate-polyacrylamide gel electrophoresis of caldesmon and other proteins that migrate anomalously. Arch. Biochem. Biophys. **297:** 46–51.

Grimberg, Å., Carlsson, A.S., Marttila, S., Bhalerao, R., and Hofvander, P. (2015). Transcriptional transitions in *Nicotiana benthamiana* leaves upon induction of oil synthesis by WRINKLED1 homologs from diverse species and tissues. BMC Plant Biol. **15:** 192.

Halford, N.G., Hey, S., Jhurreea, D., Laurie, S., McKibbin, R.S., Paul, M., and Zhang, Y. (2003). Metabolic signalling and carbon partitioning: role of Snf1-related (SnRK1) protein kinase. J. Exp. Bot. **54:** 467–475.

Hedbacker, K., and Carlson, M. (2008). SNF1/AMPK pathways in yeast. Front. Biosci. **13:** 2408–2420.

Hua, Z., and Vierstra, R.D. (2011). The cullin-RING ubiquitin-protein ligases. Annu. Rev. Plant Biol. **62:** 299–334.

Kelly, A.A., van Erp, H., Quettier, A.L., Shaw, E., Menard, G., Kurup, S., and Eastmond, P.J. (2013). The sugar-dependent1 lipase limits triacylglycerol accumulation in vegetative tissues of Arabidopsis. Plant Physiol. **162:** 1282–1289.

Kinoshita, E., Kinoshita-Kikuta, E., Takiyama, K., and Koike, T. (2006). Phosphate-binding tag, a new tool to visualize phosphorylated proteins. Mol. Cell. Proteomics **5:** 749–757.

Koo, A.J., Ohlrogge, J.B., and Pollard, M. (2004). On the export of fatty acids from the chloroplast. J. Biol. Chem. **279:** 16101–16110.

Laurie, S., McKibbin, R.S., and Halford, N.G. (2003). Antisense SNF1-related (SnRK1) protein kinase gene represses transient activity of an α-amylase (α-Amy2) gene promoter in cultured wheat embryos. J. Exp. Bot. **54:** 739–747.

Li, Y., et al. (2011). AMPK phosphorylates and inhibits SREBP activity to attenuate hepatic steatosis and atherosclerosis in diet-induced insulin-resistant mice. Cell Metab. **13:** 376–388.

Liu, J., Perumal, N.B., Oldfield, C.J., Su, E.W., Uversky, V.N., and Dunker, A.K. (2006). Intrinsic disorder in transcription factors. Biochemistry **45:** 6873–6888.

Ma, W., Kong, Q., Mantyla, J.J., Yang, Y., Ohlrogge, J.B., and Benning, C. (2016). 14-3-3 protein mediates plant seed oil biosynthesis through interaction with AtWRI1. Plant J. **88:** 228–235.

Ma, W., Kong, Q., Grix, M., Mantyla, J.J., Yang, Y., Benning, C., and Ohlrogge, J.B. (2015). Deletion of a C-terminal intrinsically disordered region of WRINKLED1 affects its stability and enhances oil accumulation in Arabidopsis. Plant J. **83:** 864–874.

Maeo, K., Tokuda, T., Ayame, A., Mitsui, N., Kawai, T., Tsukagoshi, H., Ishiguro, S., and Nakamura, K. (2009). An AP2-type transcription factor, WRINKLED1, of *Arabidopsis thaliana* binds to the AW-box sequence conserved among proximal upstream regions of genes involved in fatty acid synthesis. Plant J. **60:** 476–487.

Maizel, A., and Weigel, D. (2004). Temporally and spatially controlled induction of gene expression in *Arabidopsis thaliana*. Plant J. **38:** 164–171.

Masaki, T., Mitsui, N., Tsukagoshi, H., Nishii, T., Morikami, A., and Nakamura, K. (2005). ACTIVATOR of Spomin:LUC1/WRINKLED1 of *Arabidopsis thaliana* transactivates sugar-inducible promoters. Plant Cell Physiol. **46:** 547–556.

Moore, B., Zhou, L., Rolland, F., Hall, Q., Cheng, W.H., Liu, Y.X., Hwang, I., Jones, T., and Sheen, J. (2003). Role of the Arabidopsis glucose sensor HXK1 in nutrient, light, and hormonal signaling. Science **300:** 332–336.

Moorhead, G., Douglas, P., Morrice, N., Scarabel, M., Aitken, A., and MacKintosh, C. (1996). Phosphorylated nitrate reductase from spinach leaves is inhibited by 14-3-3 proteins and activated by fusicoccin. Curr. Biol. **6:** 1104–1113.

Muranaka, T., Banno, H., and Machida, Y. (1994). Characterization of tobacco protein kinase NPK5, a homolog of *Saccharomyces cerevisiae* SNF1 that constitutively activates expression of the glucose-repressible SUC2 gene for a secreted invertase of *S. cerevisiae*. Mol. Cell. Biol. **14:** 2958–2965.

Nakagawa, T., et al. (2007). Improved Gateway binary vectors: high-performance vectors for creation of fusion constructs in transgenic analysis of plants. Biosci. Biotechnol. Biochem. **71:** 2095–2100.

Nallamsetty, S., and Waugh, D.S. (2007). A generic protocol for the expression and purification of recombinant proteins in *Escherichia coli* using a combinatorial His6-maltose binding protein fusion tag. Nat. Protoc. **2:** 383–391.

Ohad, N., and Yalovsky, S. (2010). Utilizing bimolecular fluorescence complementation (BiFC) to assay protein–protein interaction in plants. In Plant Developmental Biology (Berlin/Heidelberg: Springer), pp. 347–358.

Pfaffl, M.W., Horgan, G.W., and Dempfle, L. (2002). Relative expression software tool (REST) for group-wise comparison and statistical analysis of relative expression results in real-time PCR. Nucleic Acids Res. **30:** e36.

Price, J., Laxmi, A., St Martin, S.K., and Jang, J.C. (2004). Global transcription profiling reveals multiple sugar signal transduction mechanisms in Arabidopsis. Plant Cell **16:** 2128–2150.

Rolland, F., and Sheen, J. (2005). Sugar sensing and signalling networks in plants. Biochem. Soc. Trans. **33:** 269–271.

Ruuska, S.A., Girke, T., Benning, C., and Ohlrogge, J.B. (2002). Contrapuntal networks of gene expression during Arabidopsis seed filling. Plant Cell **14:** 1191–1206.

Sanjaya, D., Durrett, T.P., Weise, S.E., and Benning, C. (2011). Increasing the energy density of vegetative tissues by diverting carbon from starch to oil biosynthesis in transgenic Arabidopsis. Plant Biotechnol. J. **9:** 874–883.

Sheen, J. (2014). Master regulators in plant glucose signaling networks. J. Plant Biol. **57:** 67–79.

Shen, W., Reyes, M.I., and Hanley-Bowdoin, L. (2009). Arabidopsis protein kinases GRIK1 and GRIK2 specifically activate SnRK1 by phosphorylating its activation loop. Plant Physiol. **150:** 996–1005.

Shirley, R.B., Kaddour-Djebbar, I., Patel, D.M., Lakshmikanthan, V., Lewis, R.W., and Kumar, M.V. (2005). Combination of proteasomal inhibitors lactacystin and MG132 induced synergistic apoptosis in prostate cancer cells. Neoplasia **7:** 1104–1111.

Sirichandra, C., Davanture, M., Turk, B.E., Zivy, M., Valot, B., Leung, J., and Merlot, S. (2010). The Arabidopsis ABA-activated kinase OST1 phosphorylates the bZIP transcription factor ABF3 and creates a 14-3-3 binding site involved in its turnover. PLoS One **5:** e13935.

Skowyra, D., Craig, K.L., Tyers, M., Elledge, S.J., and Harper, J.W. (1997). F-box proteins are receptors that recruit phosphorylated substrates to the SCF ubiquitin-ligase complex. Cell **91:** 209–219.

Smeekens, S., Ma, J., Hanson, J., and Rolland, F. (2010). Sugar signals and molecular networks controlling plant growth. Curr. Opin. Plant Biol. **13:** 274–279.

Tanner, S., Shu, H., Frank, A., Wang, L.C., Zandi, E., Mumby, M., Pevzner, P.A., and Bafna, V. (2005). InsPecT: identification of posttranslationally modified peptides from tandem mass spectra. Anal. Chem. **77:** 4626–4639.

Tasaki, T., Sriram, S.M., Park, K.S., and Kwon, Y.T. (2012). The N-end rule pathway. Annu. Rev. Biochem. **81:** 261–289.

Tsai, A.Y., and Gazzarrini, S. (2012). AKIN10 and FUSCA3 interact to control lateral organ development and phase transitions in Arabidopsis. Plant J. **69:** 809–821.

Vierstra, R.D. (2009). The ubiquitin-26S proteasome system at the nexus of plant biology. Nat. Rev. Mol. Cell Biol. **10:** 385–397.

Williams, S.P., Rangarajan, P., Donahue, J.L., Hess, J.E., and Gillaspy, G.E. (2014). Regulation of Sucrose non-Fermenting Related Kinase 1 genes in *Arabidopsis thaliana*. Front. Plant Sci. **5:** 324.

Xiong, Y., and Sheen, J. (2012). Rapamycin and glucose-target of rapamycin (TOR) protein signaling in plants. J. Biol. Chem. **287:** 2836–2842.

Yang, Y., Munz, J., Cass, C., Zienkiewicz, A., Kong, Q., Ma, W., Sedbrook, J., and Benning, C.; Sanjaya. (2015). Ectopic expression of WRINKLED1 affects fatty acid homeostasis in *Brachypodium distachyon* vegetative tissues. Plant Physiol. **169:** 1836–1847.

Zhou, G., et al. (2001). Role of AMP-activated protein kinase in mechanism of metformin action. J. Clin. Invest. **108:** 1167–1174.